REPORT DOCUMENTATION PAGE

1a. REPORT SECURITY CLASSIFICATION Unclassified	1b. RESTRICTIVE MARKINGS
2a. SECURITY CLASSIFICATION AUTHORITY	3. DISTRIBUTION/AVAILABILITY OF REPORT Approved for public release; distribution is unlimited.
2b. DECLASSIFICATION/DOWNGRADING SCHEDULE	
4. PERFORMING ORGANIZATION REPORT NUMBER(S)	5. MONITORING ORGANIZATION REPORT NUMBER(S)
6a. NAME OF PERFORMING ORGANIZATION Naval Postgraduate School 6b. OFFICE SYMBOL (*If applicable*) ME	7a. NAME OF MONITORING ORGANIZATION Naval Postgraduate School
6c. ADDRESS (*City, State, and ZIP Code*) Monterey, CA 93943-5000	7b. ADDRESS (*City, State, and ZIP Code*) Monterey, CA 93943-5000
8a. NAME OF FUNDING/SPONSORING ORGANIZATION 8b. OFFICE SYMBOL (*If applicable*)	9. PROCUREMENT INSTRUMENT IDENTIFICATION NUMBER
8c. ADDRESS (*City, State, and ZIP Code*)	10. SOURCE OF FUNDING NUMBERS Program Element No. / Project No. / Task No. / Work Unit Accession Number

11. TITLE (*Include Security Classification*)
CONVECTIVE HEAT TRANSFER FROM DISCRETE HEAT SOURCES IN A LIQUID FILLED VERTICAL CHANNEL

12. PERSONAL AUTHOR(S) Ronald G. Rahall

13a. TYPE OF REPORT	13b. TIME COVERED	14. DATE OF REPORT (*year, month, day*)	15. PAGE COUNT
Master's Thesis	From To	December 1992	72

16. SUPPLEMENTARY NOTATION
The views expressed in this thesis are those of the author and do not reflect the official policy or position of the Department of Defense or the U.S. Government.

17. COSATI CODES			18. SUBJECT TERMS (*continue on reverse if necessary and identify by block number*)
FIELD	GROUP	SUBGROUP	opposed mixed convection, aiding mixed convection, liquid cooling vertical channel flow

19. ABSTRACT (*continue on reverse if necessary and identify by block number*)

Natural, mixed and forced convection liquid cooling of discrete heat sources in a vertical channel were investigated experimentally. Ten heat sources were flush mounted to one side of a channel wall, while the opposite wall was unheated. Measurments of heater surface temperatures were made for a channel Reynolds number range of 0 - 1700 and heat flux range of 1050 - 4500 W/m^2. In the mixed convection regime, both aiding and opposed flow were examined. Temperature patterns on the heated surface were visualized using liquid crystal.

20. DISTRIBUTION/AVAILABILITY OF ABSTRACT	21. ABSTRACT SECURITY CLASSIFICATION	
☒ UNCLASSIFIED/UNLIMITED ☐ SAME AS REPORT ☐ DTIC USERS	Unclassified	
22a. NAME OF RESPONSIBLE INDIVIDUAL Yogendra Joshi	22b. TELEPHONE (*Include Area code*) 646-3400	22c. OFFICE SYMBOL ME/Jo

Approved for public release; distribution is unlimited.

CONVECTIVE HEAT TRANSFER FROM DISCRETE HEAT SOURCES IN A LIQUID FILLED VERTICAL CHANNEL

by

Ronald G. Rahall
Lieutenant Commander, United States Navy
B.S., United States Naval Academy, 1979

Submitted in partial fulfillment
of the requirements for the degree of

MASTER OF SCIENCE IN MECHANICAL ENGINEERING

from the

ABSTRACT

Natural, mixed and forced convection liquid cooling of discrete heat sources in a vertical channel were investigated experimentally. Ten heat sources were flush mounted to one wall of a water filled channel, while the opposite wall was unheated. Measurements of heater surface temperatures were made for a channel Reynolds number range of 0 - 1700 and heat flux range of 1050 - 4500 W/m^2. In the mixed convection regime, both aiding and opposed flow were examined. Temperature patterns on the heated surface were visualized using liquid crystals.

TABLE OF CONTENTS

LIST OF FIGURES

LIST OF TABLES

NOMENCLATURE

a - half channel thickness (m)

A_c - cross sectional area of channel (0.002 m^2)

A_s - heater surface area (0.002 m^2)

D_H - hydraulic diameter of channel (0.019 m)

g - acceleration due to gravity (9.81 m/s^2)

Gr^* - flux based Grashof number

h - heat transfer coefficient ($W/m^2 \cdot K$)

κ - thermal conductivity ($W/m \cdot K$)

L - heater strip width (0.01 m)

l_e - axial length for fully developed flow

Nu - Nusselt number

P - inside channel perimeter (0.42 m)

Pr - Prandtl number

q'' - heat flux (W/m^2)

R - resistance (Ohm)

Re - Reynolds number based on hydraulic diameter

T_{HTR} - heater strip center temperature (C)

T_{IN} - average inlet temperature (C)

ΔT - average temperature difference $T_{HTR}-T_{IN}$ (C)

U_m - mean velocity (m/s)

V_{Tot} - voltage drop across heater and precision resistor combination (Volts)

V_{Heat} - voltage drop across heater strip (Volts)

β - coefficient of volumetric expansion (K^{-1})

Θ - nondimensional temperature

ν - kinematic viscosity of water at T_{IN} (m^2/s)

ACKNOWLEDGMENT

To those who helped contribute to the success and completion of this thesis.

Professor Joshi, who provided an extra hand on the tiller when the seas got rough and helped steer me clear of shoal water.

Jim Scholfield and Tom Christian, whose diligent efforts provided the voyage repairs to keep the experiment running.

My wife, Mary Etta, and daughters, Bethany and Brianna, whose love and compassion made coming home these past two years a true safe harbor for this weary sailor.

I. INTRODUCTION

A. ELECTRONIC COOLING

With the invention of the transistor in 1947, the present computer age was born. The limit on computer design was circuit technology. As this technology grew and engineers developed ways to pack more devices on each chip, heat dissipation became a limiting design factor.

Efficient heat dissipation from highly packed circuits is vital to reliable chip operation. For every 10°C rise in junction temperature above 85°C, reliability suffers by a factor of two [Ref 1: p. 35]. The importance of adequate cooling is better visualized by considering a typical 5 mm by 5 mm chip dissipating 10 W of power. This gives an average heat flux of 4×10^5 W/m^2--just two orders of magnitude less than that on the sun's surface.

Electronic cooling is evolving with advances in semiconductor fabrication technology. As Small Scale Integration (SSI) has developed into Ultra Large Scale Integration (ULSI), so has air cooling technology developed into conduction and direct liquid cooling.

1. Air Cooling Technology

For low power densities, air cooling is commonly used to cool electronic components. Within air cooling technology,

the simplicity of natural convection has given way to sophisticated forced convection designs in order to dissipate the heat from high power systems.

In order to enhance heat removal capabilities, designers have had to rethink module and system designs. The Hitachi SiC RAM and IBM 4301 modules are two examples [Ref 2: p. 294]. These designs have attempted to minimize internal and external heat flow resistances across the module as well as made use of parallel flow schemes to reduce the temperature rise across the system. In addition to the above, other enhancement techniques being explored and used include: impinging air flow schemes, turbulators, and water-cooled "interboard" heat exchangers [Ref 2: pp. 293-296].

While much has been done to enhance air cooling technology, these developments have failed to keep pace with the heat dissipation requirements of modern electronic equipment.

2. Conduction Cooling Technology

IBM's Thermal Conduction Module (TCM) is an example of keeping pace with today's higher power densities. The key elements in this technology include: a modular cold plate subsystem, a coolant distribution loop, heat rejection loop and appropriate thermal sensing and control hardware [Ref 2: p. 298]. Briefly, the heat path goes from the chip surface through a spring loaded piston and housing to the cold plate.

Enhancements to this technology center around reducing the thermal resistance and include: optimum geometry of the piston, housing and cold plate; improved thermal fillers across physical gaps; and optimum flow rates. [Ref 2: pp. 298-299].

A promising enhancement technique which can be classified as either conduction or direct cooling is the microgroove/microchannel technique. First proposed by Tuckerman and Pease [Ref 3: pp. 126-129], this technique would significantly reduce the conductive resistances. The cold plate, in effect, is brought to the under side of the integrated circuit chip.

3. Direct Liquid Cooling

Because of higher density and specific heat of liquids compared to gases, liquid immersion cooling has a clear heat transfer rate advantage over air cooling technology. Immersion and circulation of coolant through microgrooves in the chip eliminate the interfacial resistance that restricts conduction cooling technology.

The Cray-2 and ETA-10 supercomputers are two examples of the use of direct liquid cooling. With the success of these systems, researchers and designers have had an increased interest in this method of cooling. New fluids are being developed to meet the strict chemical, electrical and thermal requirements. Additionally, as with any new technology, a

knowledge base of data is beginning to be developed. Although much research has been conducted for air cooling, relatively less has been done with direct liquid cooling. Due to the large differences in the thermophysical properties, the air cooling data in the literature is not directly applicable to liquid cooling. The modes of direct liquid cooling are: natural, forced and mixed convection; phase change; falling film; and jet impingement.

B. PREVIOUS RESEARCH ON SINGLE PHASE LIQUID COOLING

In this section and the one following, a brief review of single phase liquid cooling for natural, forced and mixed convection is presented. In order to establish a knowledge base, it is conventional to start with simple configurations, attempt to fully understand the behavior observed and then expand this understanding to more complicated situations by both computer simulation and further experimentation. For natural, mixed and forced convection, typical configurations simulating electronic cooling applications include channels, isolated surface and full or partial enclosures.

Park and Bergles have investigated natural convection for discrete heat sources on isolated surfaces [Ref 4: pp. 90-96]. By varying heater size and arrangements they found that shorter, wider heaters provided higher heat transfer coefficients; protruding heaters performed better than flush mounted heaters; downstream heater heat transfer coefficients

were lower than upstream ones; and staggered vice in line configuration was better for heat transfer.

Joshi and Kelleher [Ref 1: pp. 35-39] have described a number of natural convection liquid immersion cooling studies for the three configurations identified above. Both experimental and computational studies are described. Applications of natural convection cooling of actual packages are addressed.

Keyhani et al. [Ref 5: pp. 616-623] considered two dimensional natural convection from eleven discrete flush mounted heat sources on a vertical wall in a rectangular enclosure. Heat transfer data and flow visualization revealed primary, secondary and tertiary flow patterns and indicated that stratification was an important factor influencing the temperature of the heated sections. These results also revealed higher Nusselt numbers for discrete heating than for a fully heated vertical wall.

Forced convection liquid cooling research has centered around the earlier work done by Tuckerman and Pease on microgroove/microchannel configurations. Kishimoto and Sasaki [Ref 6: p. 358] proposed methods to reduce temperature variations across silicon chips by using diamond shaped channels. Phillips et al. [Ref 7: pp. 227-248] provide models for heat transfer and pressure drops for various aspect ratio channels for laminar and turbulent flow regimes. Phillips

[Ref 8: pp. 31-48] also presented a thermal resistance model for predicting microchannel cooling performance.

C. MIXED CONVECTION

In many applications, both natural and forced convection are important. Mixed convection deals with the flow regime where characteristic buoyant and forced convection velocities are comparable. The effects of buoyancy forces and the specific parametric ranges where they become important in the overall heat transfer process are highly dependent on the geometry and boundary conditions.

Mixed convection combines the natural and forced flow effects in the form Gr/Re^n, where the Grashof number (Gr) is a measure of the ratio of buoyancy to viscous forces and Reynolds number (Re) indicates the ratio of inertia to viscous forces. The exponent 'n' is a function of geometry, fluid, and heating condition. As this nondimensional ratio approaches zero, forced convection dominates; as it approaches infinity, natural convection dominates. Mixed convection may be aiding or opposed. Aiding implies free stream flow in the direction of buoyancy forces; opposed convection implies free stream flow opposite to buoyancy forces.

Cheng et al. [Ref 9: p. 375] obtained analytical solutions for buoyancy-assisted, fully developed laminar mixed convection flow in a channel for three combinations of thermal boundary conditions--isoflux-isoflux, isoflux-isothermal and

isothermal-isothermal. For these conditions, effects of flow reversal and heat transfer characteristics were studied.

Maheny, Incropera and Ramadhyani studied, experimentally and numerically, mixed convection from an in-line, four row array of twelve discrete, square, flush mounted heat sources in a liquid filled horizontal channel. They determined the variations of row-average Nusselt vs Reynolds number and found that heat transfer may be enhanced due to buoyancy effects thereby reducing the required pumping power. [Ref 10: pp. 1233-1243]

Mori and Ohbuchi performed experiments on the dependence of heat transfer on heat flux for downward flows in a vertical straight circular tube for Reynolds numbers less than 2000. Their study showed that for small heat fluxes the temperature and velocity gradients at the tube wall were decreased by buoyancy forces and that heat transfer was reduced. At higher heat fluxes, buoyancy and velocity fluctuations appeared at Re > 500 resulting in enhancemented heat transfer. [Ref 11: pp. 1231-1237]

D. OBJECTIVES OF PRESENT STUDY

This study experimentally investigated natural, mixed and forced convection heat transfer in a water filled vertical rectangular channel with discrete heater strips on one wall. Specific objectives were:

- To investigate natural convection effects and compare the heat transfer data with known correlations.
- To investigate heat transfer characteristics for opposed mixed convection.
- To investigate heat transfer characteristics for aiding mixed convection.

II. EXPERIMENTAL APPARATUS

A. TEST CHANNEL ASSEMBLY

The test channel assembly is similar to the one used by Syring. [Ref 12] It consists of three main systems: fluid circulation; power distribution; and data acquisition (Figure 1).

1. Fluid Circulation System

Water is circulated in a closed system consisting of: a vertical rectangular channel and associated tubing; positive displacement pump; and flow meter. The vertical channel consists of two 1 cm thick plexiglass boards 2.0 m by 0.25 m separated by a 1 cm thick plexiglass spacer with a 2.5 cm wide and 1 mm thick rubber gasket. At the top and bottom of the channel are surge tanks. Within the channel are the test section and two flow straightening regions. The top flow straightening region (encountered by the flow prior to reaching the test section during opposed mixed convection) is located 1.0 m above the top of the test section. The other region used for conditioning the flow during the aiding convection studies is located 0.3 m below the bottom of the test section.

The test section constitutes a 20 cm x 19 cm portion of one wall of the vertical channel. Ten 0.5 cm x 20 cm and

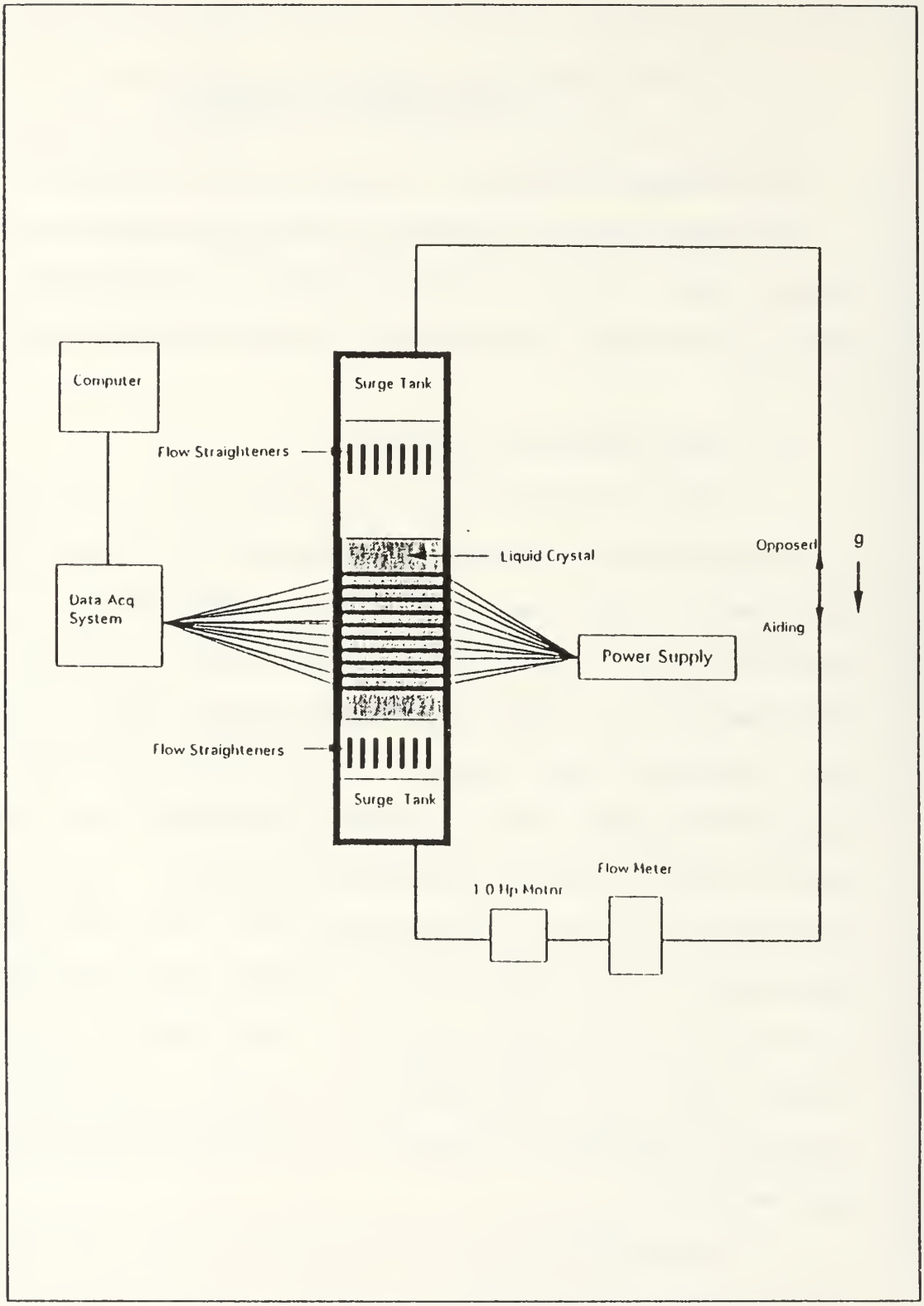

Figure 1. Overall schematic of experimental apparatus.

0.120 cm deep grooves were milled horizontally across the test surface at spacings of 1 cm. These grooves served as thermocouple beds for each heating strip. A second set of ten, wider but shallower, grooves (1.0 cm x 20 cm and 0.08 cm deep) were milled on top of each of the thermocouple grooves. These grooves housed the flush mounted heating strips. An example of a typical heating groove surface is shown in Figure 2. Finally, a vertical 1.4 cm x 29 cm and 0.120 cm deep groove was milled to house the electrical leads from the ten heater strips. A front view of the test surface is shown in Figure 3. A side view of the channel is shown in Figure 4. Before mounting the heater strips to the plexiglass, five copper-constantan (Cu-Co) thermocouples were mounted in the deepest groove for each heater. This resulted in a total of fifty thermocouples for the entire test section. Thermocouples for each heater were spaced as shown in Figure 3. The two end thermocouples for each heater were made with 0.254 mm diameter wire; the middle three were made from 0.127 mm diameter wire.

All of the thermocouples were mounted using a low thermal conductivity fast curing exopy (Omega bond 100). This served to effectively reduce the conduction losses across the plexiglass. A very thin layer of a high thermal conductivity epoxy (Omega bond 101) was placed in the area of the heating strips where the thermocouples would be measuring. The heating strips were then carefully mounted in their respective

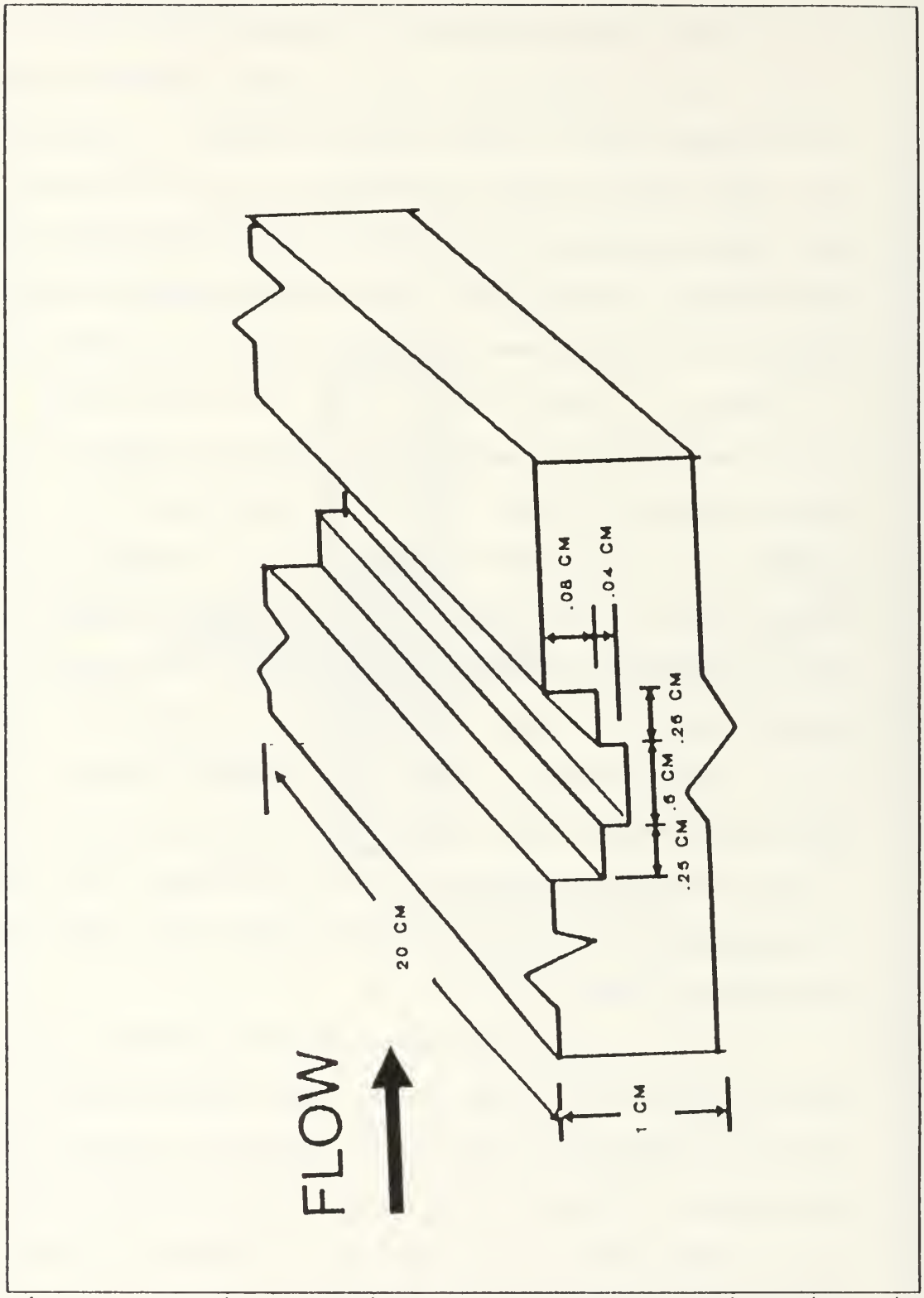

Figure 2. Typical heating surface groove. Dimensions in cm.

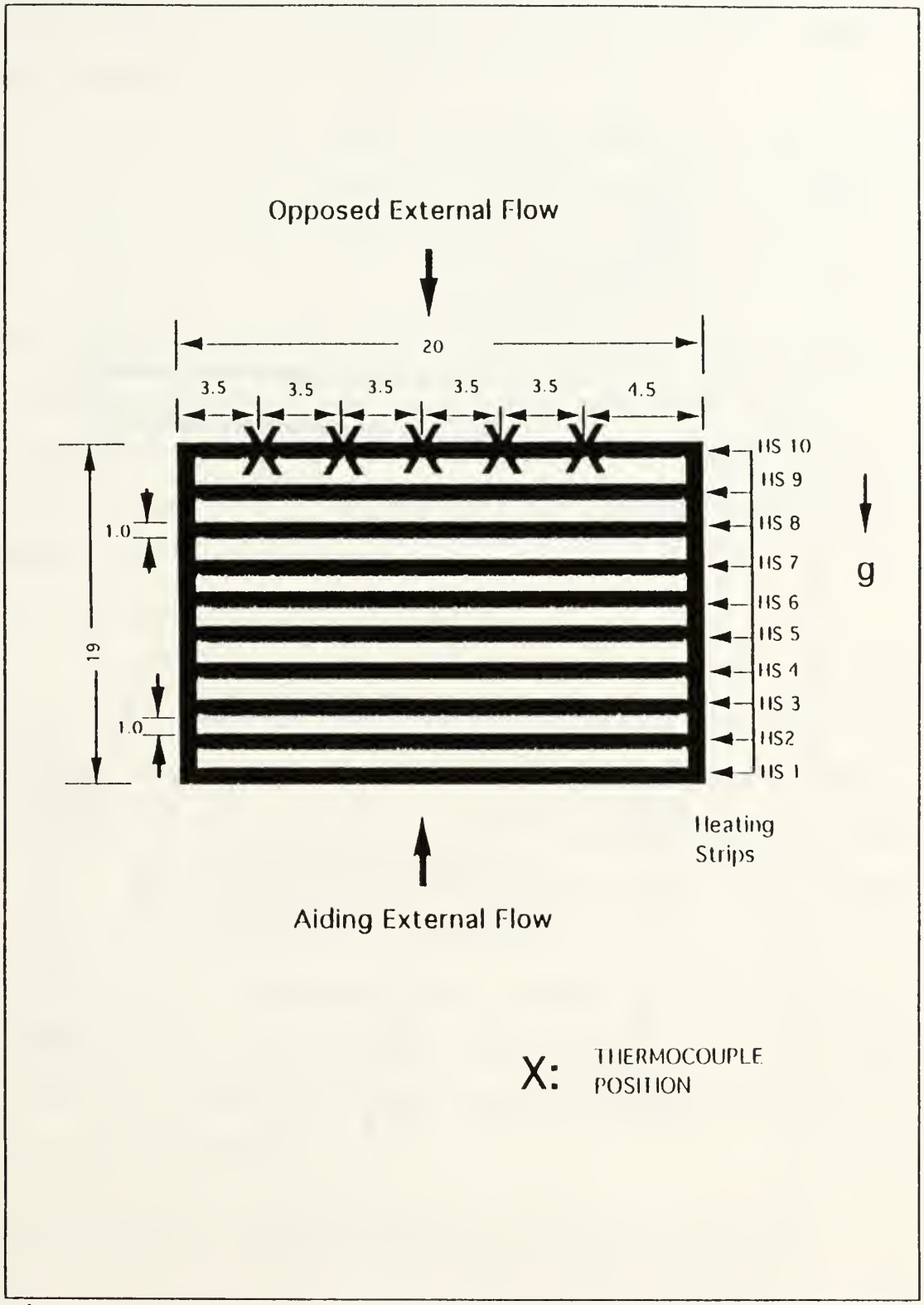

Figure 3. Front view of test surface. Dimensions in cm.

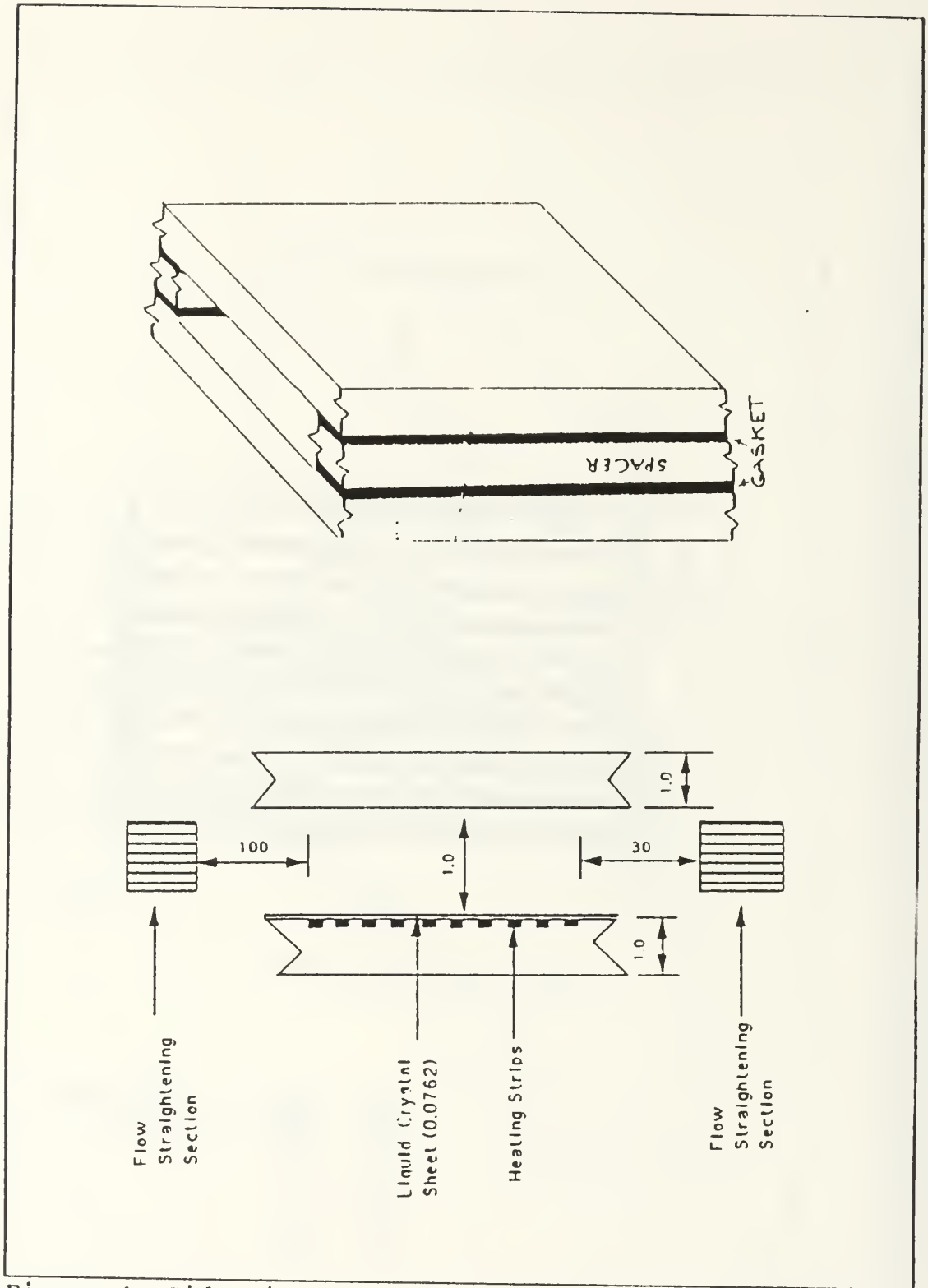

Figure 4. Side view of test surface. Dimensions in cm.

grooves using a very thin coat of Omega bond 100 to ensure a flush mounted heating surface.

A Cole-Parmer positive displacement gear type pump driven by a variable speed motor produced Reynolds numbers in the range of interest (0 to 1700). An Omega turbine flow meter was used to monitor the fluid flow rates. The flow meter was calibrated by comparing its output to measurements of quantities of water collected over specified times. The maximum uncertainty in flow rate was 0.5%. Teflon fittings and tubing provided the connections between the vertical channel, pump and flow meter.

2. Power Distribution System

A schematic of the power distribution panel is shown in Figure 5. Power to the individual heaters was supplied by a Hewlett Packard HP 6269B, 0-40 VDC, 0-50 A power supply. This supply was connected to a common bus which provided power to each of the ten heating strips. Each heater was connected in series with a precision resistor ($R = 2.01 \pm 0.005\ \Omega$). The data acquisition system obtained voltage readings across the entire bus bar (V_{Tot}) and across each heater (V_{Heat}). From these two measured values, the input power was computed using the following relationship:

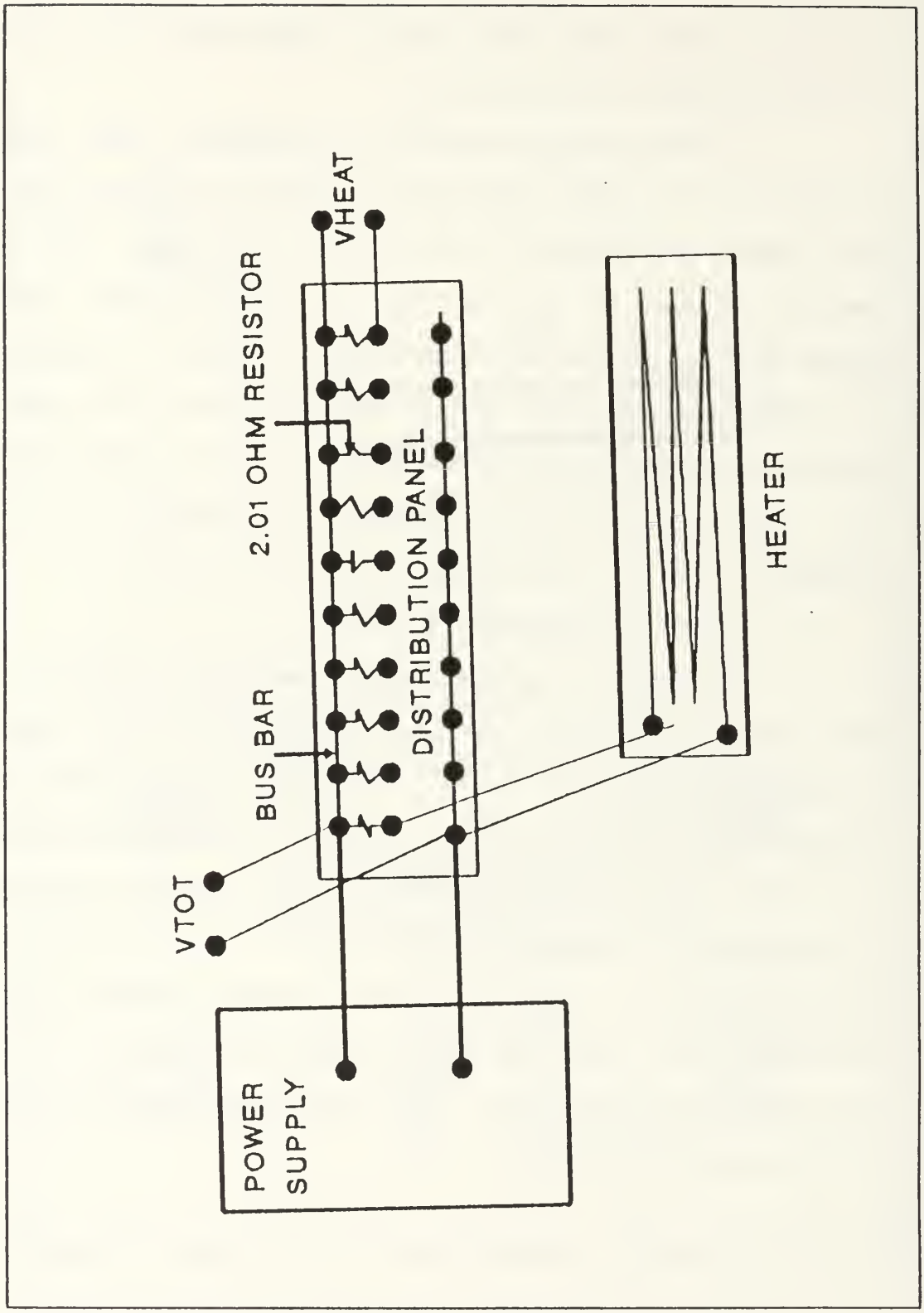

Figure 5. Power distribution system.

$$Power = \left(\frac{V_{Tot} - V_{Heat}}{R} \right) * V_{Heat}$$

3. Data Acquisition Assembly

The data acquisition system consisted of a HP 9000 computer and a HP 3852 data acquisition unit. The computer instructed the data acquisition system to monitor temperatures from desired thermocouples and measure the power delivered to each heater strip. Only selected thermocouples were scanned for each data run, depending upon the information desired. The thermocouples were scanned one at a time at a sampling rate of 5 samples/second.

B. LIQUID CRYSTALS

The surface temperature patterns were visualized using a 0.762 mm thick, 20 cm X 20 cm, Hallcrest thermochromic liquid crystal (TLC) sheet bonded to the test surface as seen in Figure 4. The crystals on this sheet displayed shades of green and blue in reaction to temperature changes in the range of 30 to 35°C. The observed color bands were compared with the average inlet temperature T_{IN}. The first appearance of green and blue corresponded to 30.5 °C and 36.0 °C respectively.

C. DISCUSSION OF SPECIAL FEATURES

Before explaining the experimental procedure in detail, a general discussion of certain design and data reduction procedures is presented.

With a fixed vertical rectangular geometry, flow rates and power inputs were varied. Mean flow velocities ranged from 0 to 0.08 m/s and heat fluxes from 1050 W/m^2 to 4500 W/m^2. With these varying conditions, experimental data runs were performed for no flow, opposed and aiding flows.

For laminar conditions, the axial length for fully developed flow, l_E, is:

$$l_E = 0.16 * a * \left(\frac{U_m * a}{\nu} \right)$$

where, U_m is the mean velocity and 'a' the channel half width [Ref 13: pp. 185-186]. This criterion is for flow between flat parallel plates. Table I provides sample entry length values for various Reynolds numbers. Based on these lengths, flow straighteners were positioned in the test channel for both the aiding and opposed mixed convection studies.

Free stream temperature (T_{IN}) was evaluated by taking the average of two Cu-Co thermocouples installed on the inlet side of each set of flow straighteners. Water properties were

TABLE I. CHANNEL ENTRY LENGTH VALUES FOR VARIOUS REYNOLDS NUMBERS

Re	GPM	U_m (m/s)	l_E (m)
500	0.7516	0.0237	0.1052
1000	1.5640	0.0493	0.2105
1500	2.2963	0.0724	0.3155
1700	2.6037	0.082	0.378

evaluated based on T_{IN}. The center temperature (T_{HTR}) was used for all heater measurements because heater strip temperature was symmetrical about the center and showed only small spanwise variation (within a 0.2°C band).

Conduction loss through the substrate to the outside environment was neglected. For a heat source where the surface area-to-perimeter is large, Baker [Ref 14: p. 172] suggests that the substrate conductivity would have a small effect on total heat transfer.

D. EXPERIMENTAL PROCEDURE

For natural convection, data were taken with only heater strip 1 energized for nine different heat fluxes (500, 1000, 1500, 2000, 2500, 3000, 3500, 4000 and 4500 W/m^2). After a steady state condition was reached, five minutes of data, sampled at a sampling frequency of 5 hz, were taken on the

center thermocouple for each flux level. This procedure was repeated for heater strips 2 and 3. A total of 27 data runs were performed.

For opposed and aiding mixed convection, all heater strips were energized at four different power levels (1050, 2500, 3500 and 4500 W/m^2) and 11 different Reynolds numbers were considered (100, 200, 300, 400, 500, 600, 800, 1000, 1200, 1500 and 1700). After a nominal steady state condition for flux and flow rate was achieved (approximately five minutes), a five minute continuous data run was performed on all center thermocouples. For a given flux level, data runs were conducted in a high to low Reynolds numbers sequence (1700 through 100). A total of 44 data runs were conducted for opposed and 44 data runs for aiding flow.

III. RESULTS

A. DATA ANALYSIS

Neglecting substrate conduction losses, a simple energy balance for each heater strip yields:

$$Q_{CONV} = Q_{Heat}$$

where,

$$Q_{Heat} = \left(\frac{V_{Tot} - V_{Heat}}{R} \right) * V_{Heat}$$

and

$$Q_{CONV} = hA_s\Delta T$$

In the above equations, h is the convective heat transfer coefficient, A_s is the heater surface area and ΔT the difference between T_{HTR} and T_{IN}.

The average Nusselt number (Nu) was calculated as:

$$Nu = \frac{h * L}{\kappa}$$

Reynolds number (Re) was calculated by:

$$Re = \frac{U_m * D_H}{\nu}$$

where, D_H is the hydraulic diameter defined as

$$D_H = \frac{4 * A_C}{P}$$

and A_C is the channel cross sectional area and P the channel perimeter.

Flux based Grashof number (Gr*) was calculated by:

$$Gr^* = \frac{g\beta q'' L^4}{\kappa \nu^2}$$

where, β is the volumetric expansion coefficient for the fluid and q″ the heat flux.

Nondimensional temperature was calculated using:

$$\Theta = \frac{\Delta T * \kappa}{q'' * L}$$

The uncertainties for Nu, Re and Gr are 5.2, 6.5 and 5.1% respectfully. Sample calculations are found in Appendix A and B.

Data reduction for this study resulted in the following plots:

- Natural convection: Nu vs Gr^*.
- Opposed mixed convection: ΔT vs Re;
  Nu vs Re; and

Θ vs Re.

- Aiding mixed convection: ΔT vs Re;

  Nu vs Re.

B. NATURAL CONVECTION RESULTS

The primary reason for looking at natural convection was to establish a level of confidence in the test apparatus and to compare present data with two published constant-heat-flux vertical wall correlations.

Figure 6 shows a comparison of the present data with Fujii and Fujii [Ref 15: p. 320] correlation for a fully heated vertical plate.

$$Nu_x = \frac{q''x}{\kappa(T_s(x)-T_\infty)} = \left(\frac{Pr}{4+9Pr^{1/2}+10Pr}\right)^{0.2} * (Gr^*_x Pr)^{0.2}$$

This correlation for the local Nusselt number applies for laminar flow along semi-infinite vertical flat plate maintained at a uniform heat flux. Also shown in Figure 6 is an experimental correlation from Joshi and Knight [Ref 16], for a single column of in line flush mounted heat sources on a vertical substrate given by $Nu=1.11*(Gr^*)^{0.12}$. The comparison is shown for heater strips 1, 2 and 3 of the present study. The local Nusselt numbers were evaluated at the heater strip vertical midpoints (0.005 mm).

The heat transfer coefficients for the heater strips were 57% below the Fujii and Fujii and 36% below the Joshi and Knight correlations. The power law exponents (n) for Nu_x = Constant*Gr_x^{*n} for References [15], [16] and this study are 0.2, 0.12 and 0.057 respectively.

The difference between Nu_x for References [15] and [16] are attributed to heater size, geometry and boundary conditions. In particular, the use of discrete heat sources in the latter and the fact that a uniform flux condition is not easily achieved with small heat sources are likely to be the primary reasons for these deviations. The present configuration differs from Reference [16] in that the heaters are much wider and also the opposite channel wall is likely to have an influence. The self-consistency of the present results is indicated by the good agreement at the three locations--HS1, 2 and 3.

C. OPPOSED MIXED CONVECTION RESULTS

Four different heat flux settings (1050, 2500, 3500 and 4500 W/m^2) and eleven Reynolds numbers between 100 and 1700 were used to analyze the heat transfer characteristics of ten discrete flush mounted heat strips in an opposed flow condition. For the initial part of this section only the odd heaters for q"=1050 W/m^2 will be discussed. However, it should be noted that the even heater strips and other heat flux settings exhibited similar trends. Plots to be presented

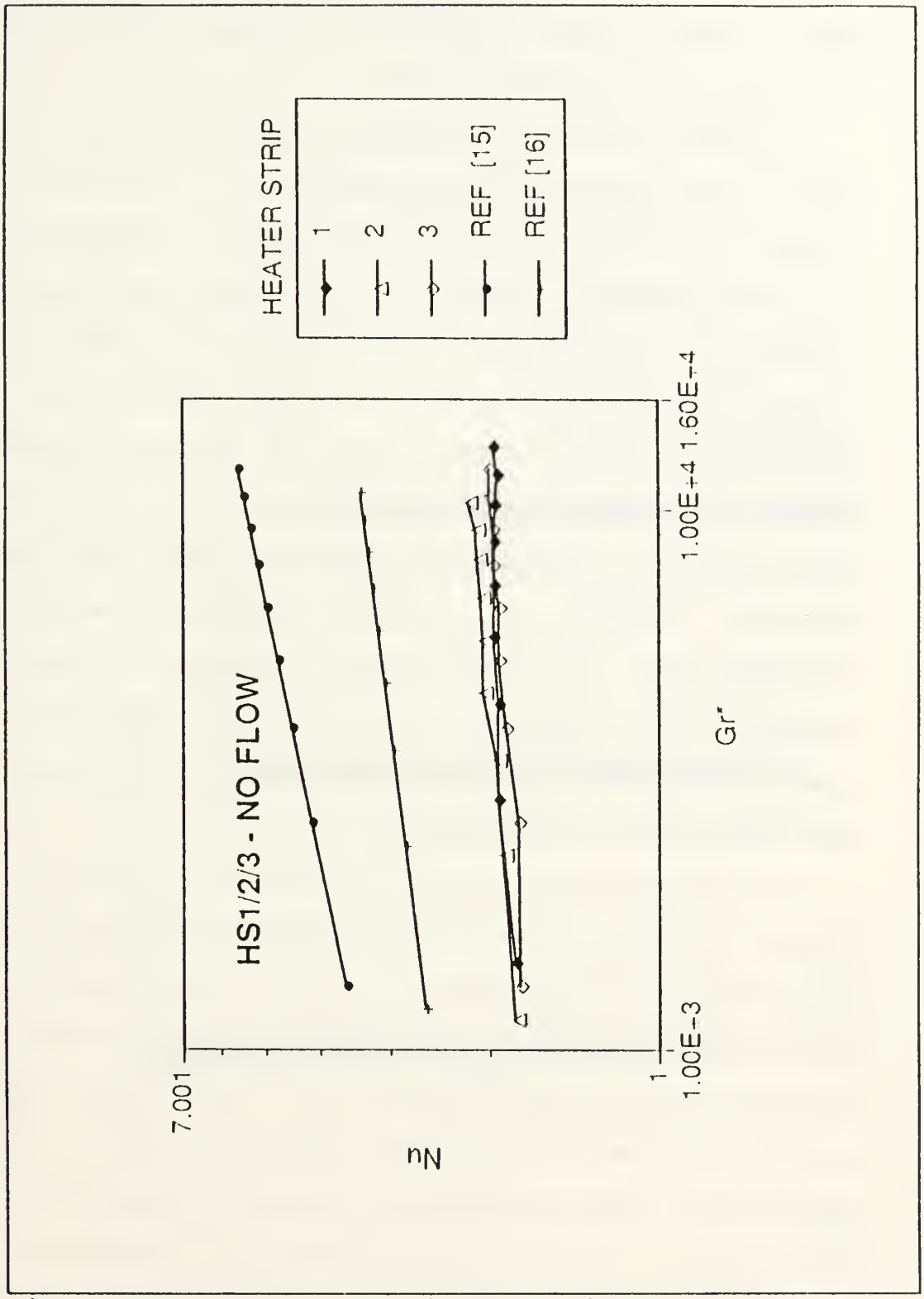

Figure 6. Natural convection comparison between Ref[15], Ref[16] and HS1,2 and 3.

are: Delta Temp (T_{HTR}-T_{IN}) vs Time; Nu vs Re; and Nondimensional Temp (Θ) vs Re.

Figures 7a-l show Delta Temp vs Time for Reynolds numbers between 1700 and 100 for odd heaters for q''=1050 W/m^2. These figures show the response of the heater temperatures with decreasing Reynolds numbers for all other parameters fixed. Figures 7a-g (Re range of 1700-500), indicate conditions where forced convection dominates. At high flow rates (Figures 7a,b), the temperature differences are collapsed together and relatively small differences between the heat transfer coefficients at the various locations exist. As flow rates decrease (Figures 7c-g), a distinct separation between heater strips is seen. The temperature difference is lower for HS9 (heater strip closest to inlet flow) but increases for HS1 (heater strip furthest from inlet flow). Additionally as Re decreases, all ΔT's increase.

For Re between 500 and 100, Figures 7h-j show opposed mixed convection effects--where buoyant and forced convection velocities are comparable. This is seen in the almost periodic oscillatory behavior of ΔT for heater strips furthest from the inlet flow (Figure 7h). As Re decreases, the oscillations becomes aperiodic (Figures 7i and j) with larger amplitudes. Other observations are the transposing of HS9 and HS1 (Figures 7i,j,k) from a minimum ΔT to maximum ΔT in the heater array and the more noticeable aperiodic oscillations of HS7 and HS9 (Figures 7i,j)--the two heater strips closest to

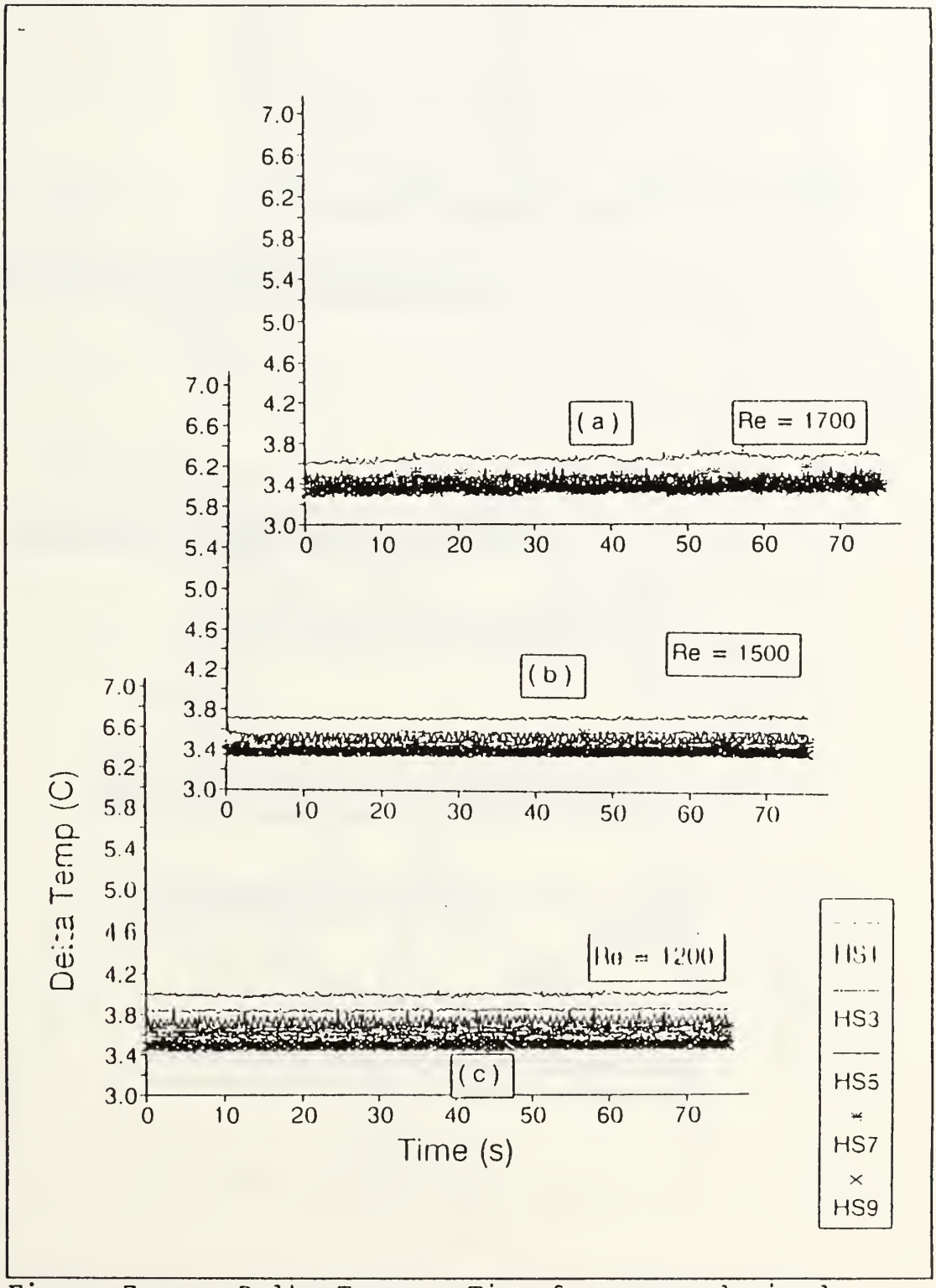

Figure 7a-c. Delta Temp vs Time for opposed mixed convection at q"=1050 W/m^2 and Re=1700-1200.

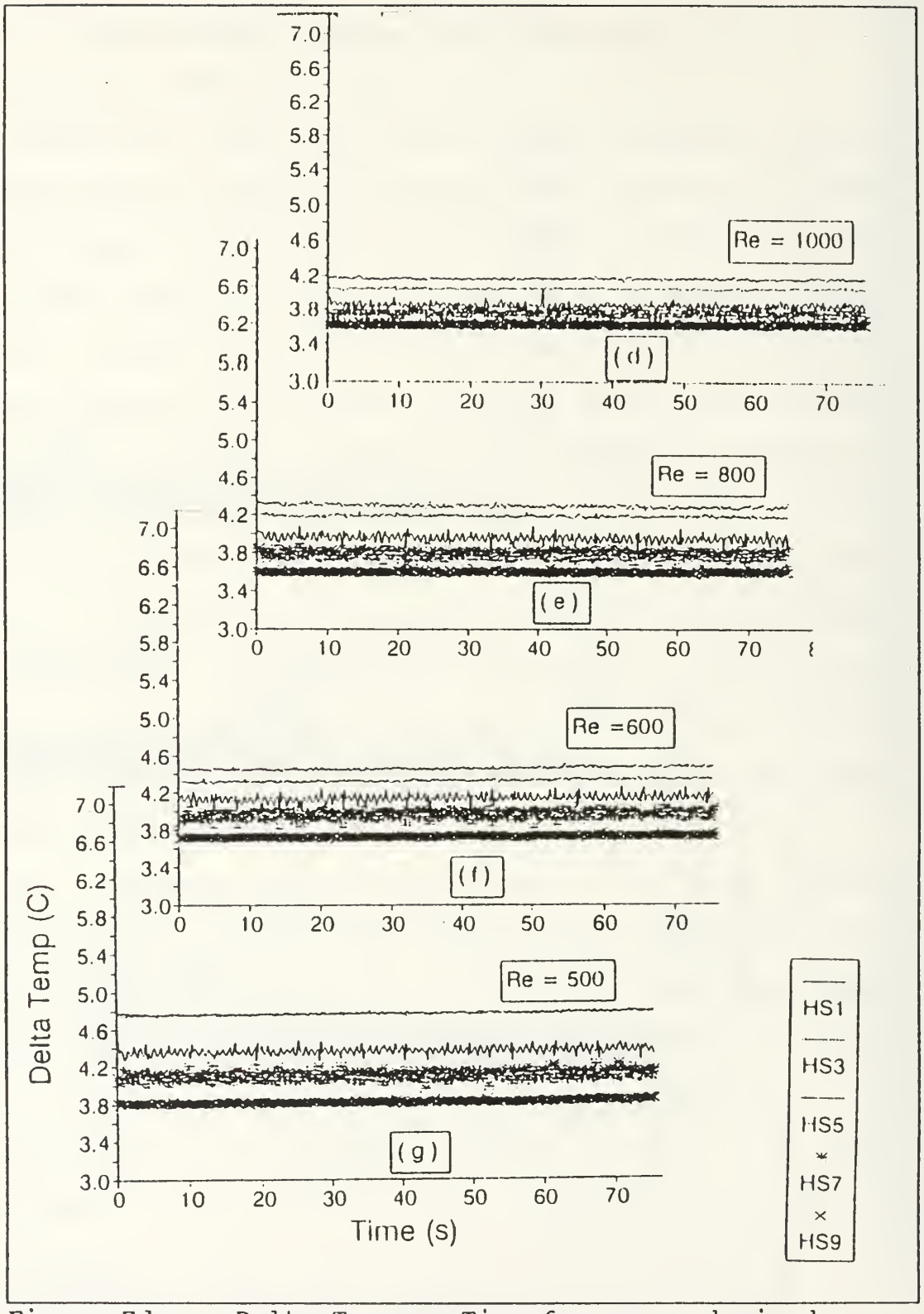

Figure 7d-g. Delta Temp vs Time for opposed mixed convection at q''=1050 W/m^2 and Re=1000-500.

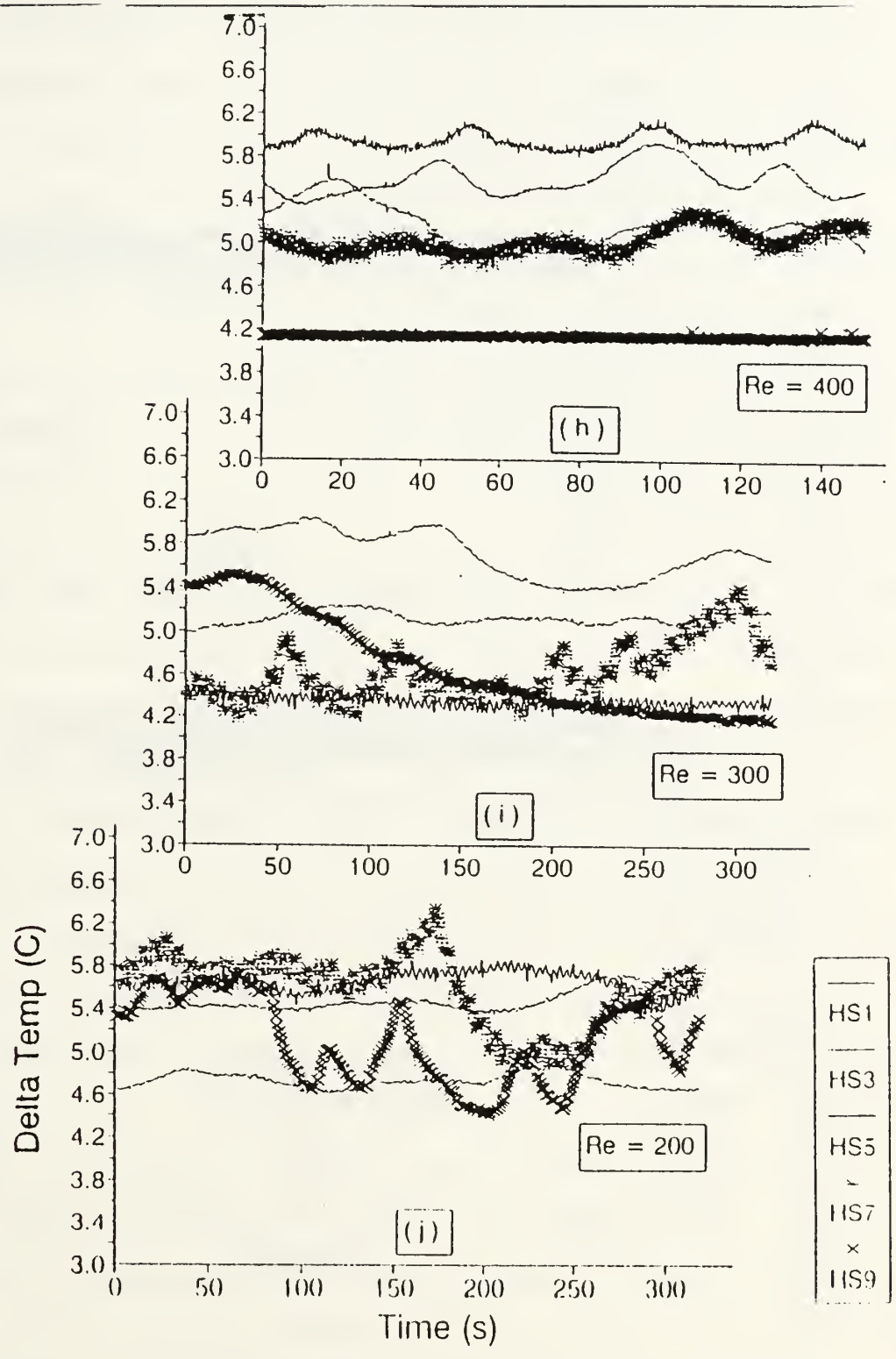

Figure 7h-j. Delta Temp vs Time for opposed mixed convection at q"=1050 W/m^2 and Re=400-200.

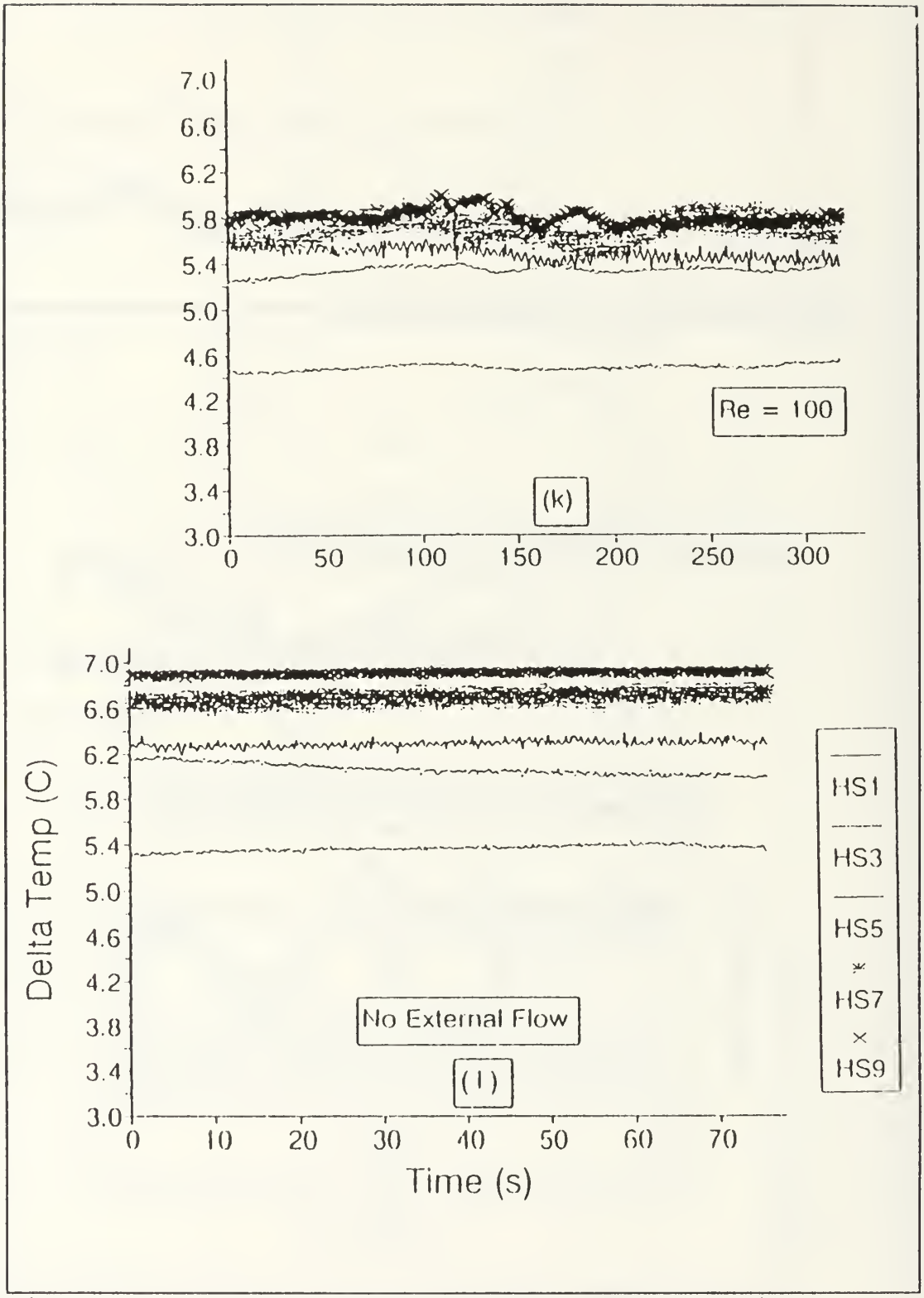

Figure 7k,l. Delta Temp vs Time for opposed mixed convection at q''=1050 W/m^2 and Re=100-0.

the inlet flow. It is very clear that buoyant and forced convection forces are competing for dominance between Re=200-500. Figures 7k and l show transport dominated by buoyancy effects and the complete transposition of HS9 and HS1.

The Nusselt number variations for heat fluxes of 1050, 2500, 3500 and 4500 W/m^2 are shown in Figures 8a-d. As observed in Figures 7a-g, a Re increase was accompanied by a decrease in ΔT. For $q'' = 1050\ W/m^2$, Figure 8a gives a better representation of this behavior in terms of Nu. For Re = 500 to 1700, Nu is higher for heater strips closest to the inlet flow, and it increases with each heater strip as Re increases. The ΔNu between HS1 and HS9 at Re=500 is 0.95; at Re=1700 it is 0.17. This is an 85% reduction and shows a collapsing of the data. Also note that HS1 and HS9 form a high/low envelope for all other heater strips. Another observation is that as Re decreases, the oscillation becomes aperiodic (Figures 7i and j) and there is a transition region were Nu shows no clear trend between Re = 200 - 500 (Figure 8a).

Comparison of the other heat fluxes shows behavior similar to Figure 8a. Heater strips 9 and 1 envelope the other heaters and there are distinct buoyant, mixed and forced convection dominated regimes. Figures 8a-d show the transition between these three regimes and Table II summarizes the mixed convection regime.

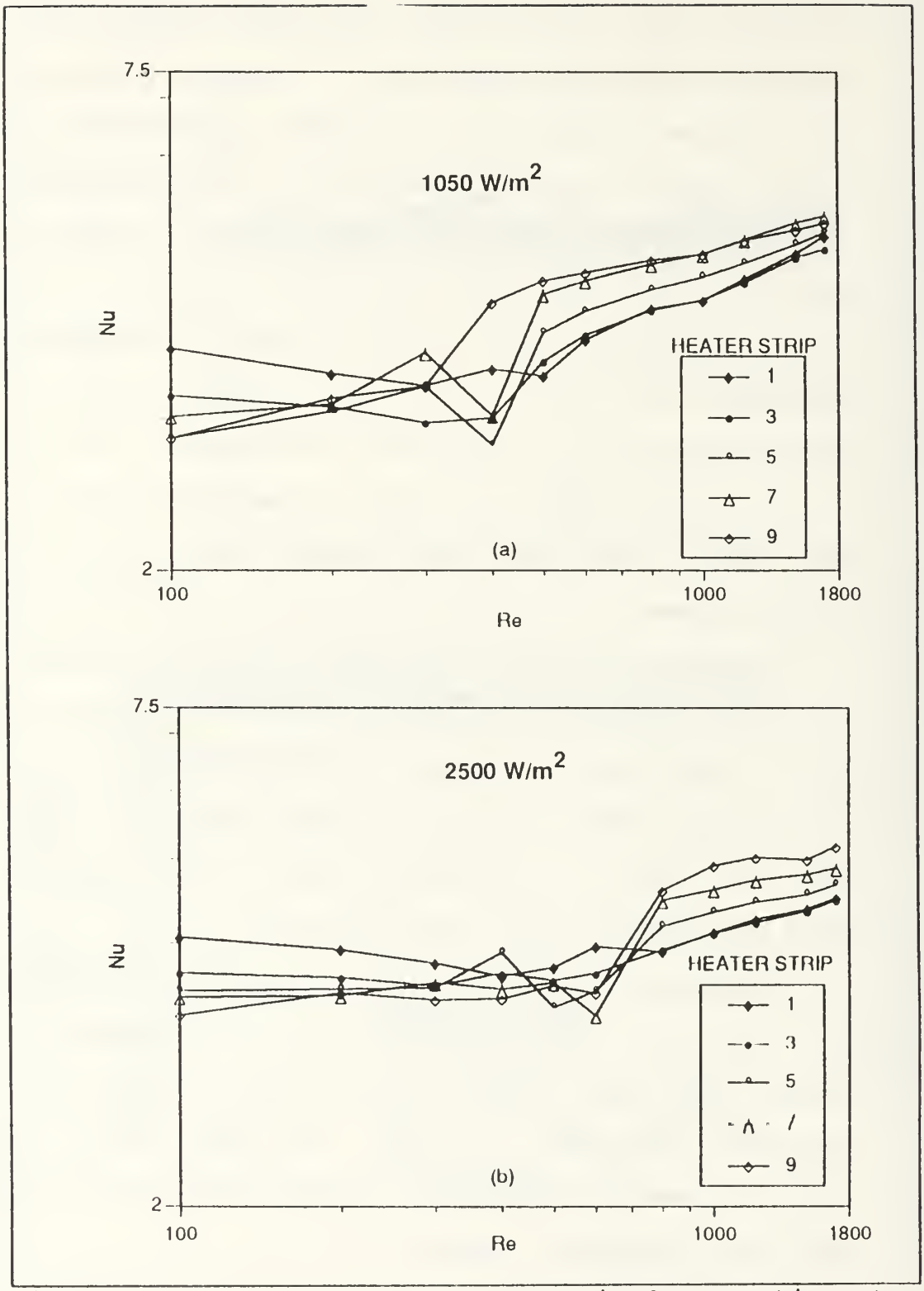

Figure 8a,b. Nu vs Re for opposed mixed convection at q"=1050 and 2500 w/m^2.

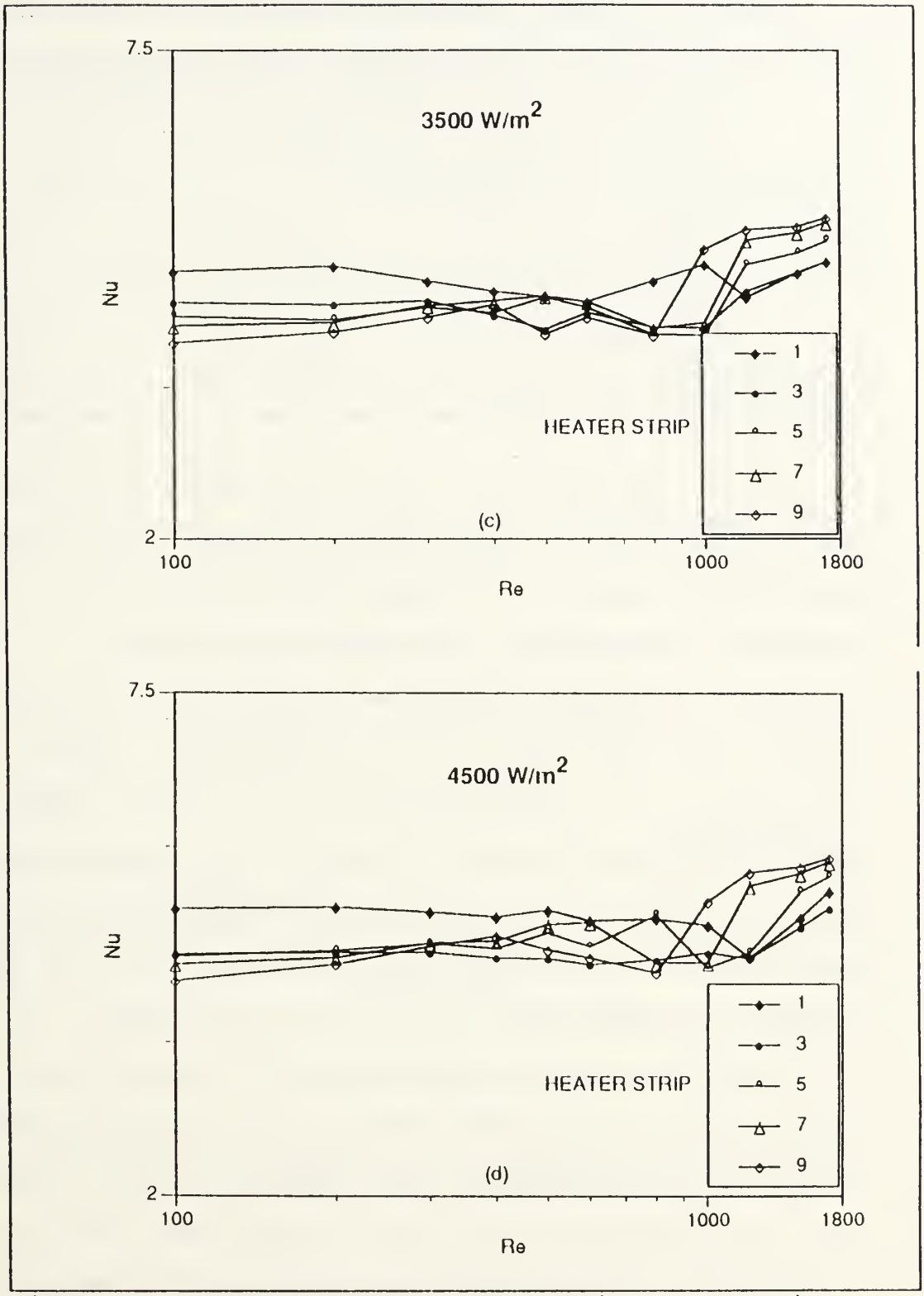

Figure 8c,d. Nu vs Re for opposed mixed convection at q''=3500 and 4500 W/m^2.

TABLE II. MIXED CONVECTION REGIME FOR OPPOSED FLOW

q'' (W/m^2)	Re range for mixed convection
1050	200 - 500
2500	300 - 800
3500	300 - 1200
4500	300 - 1500

It is also interesting to note the transposition of HS1 and HS9 in Figures 8a-d. HS1 has the highest Nu at low Re, but the lowest at high Re. The opposite is true for HS9. This is reasonable considering the downstream effects of a row of heaters. In buoyancy dominated regions, Nu for HS1 will be greater than HS9 due to the increasing thermal energy convected by the flow resulting in higher temperatures downstream (flow from HS1 to HS9). In a forced convection dominated regime, Nu for HS9 will be greater than HS1 due to the reversal in the direction of the bulk flow (flow from HS9 to HS1). Figures 8a-d clearly show these trends.

The nondimensional temperatures (Θ), Figures 9a-d, clearly illustrate the transition between the transport regimes by displaying the temperature oscillations at HS1 and HS10 for the four different heat fluxes. Note that the cross over point shifts right as heat flux increases and that the heater strip temperature oscillations occur within the Re bands shown

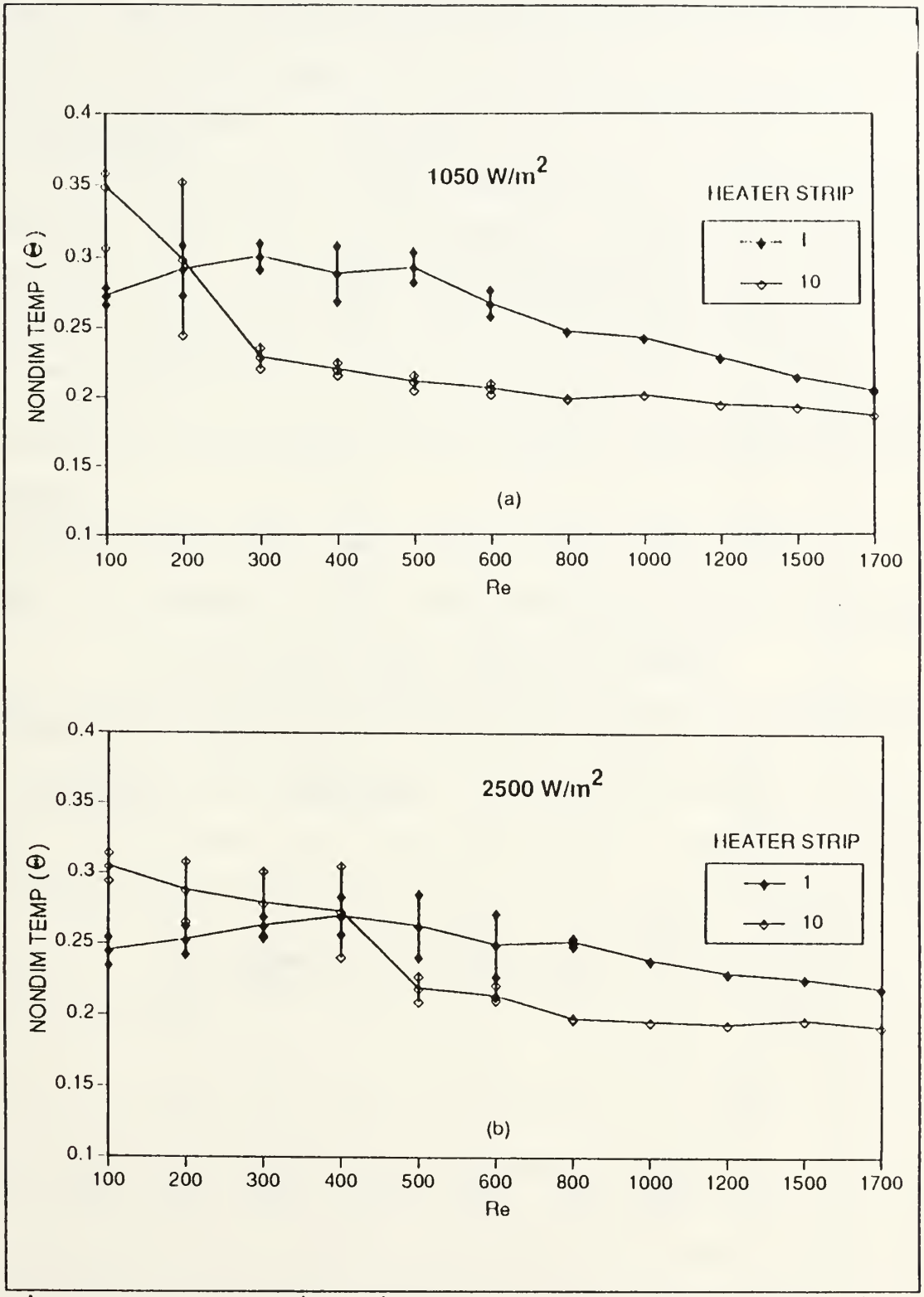

Figure 9a,b. Nondimensional Temp vs Re for opposed mixed convection at HS1 and 10 for q"=1050 and 2500 W/m^2.

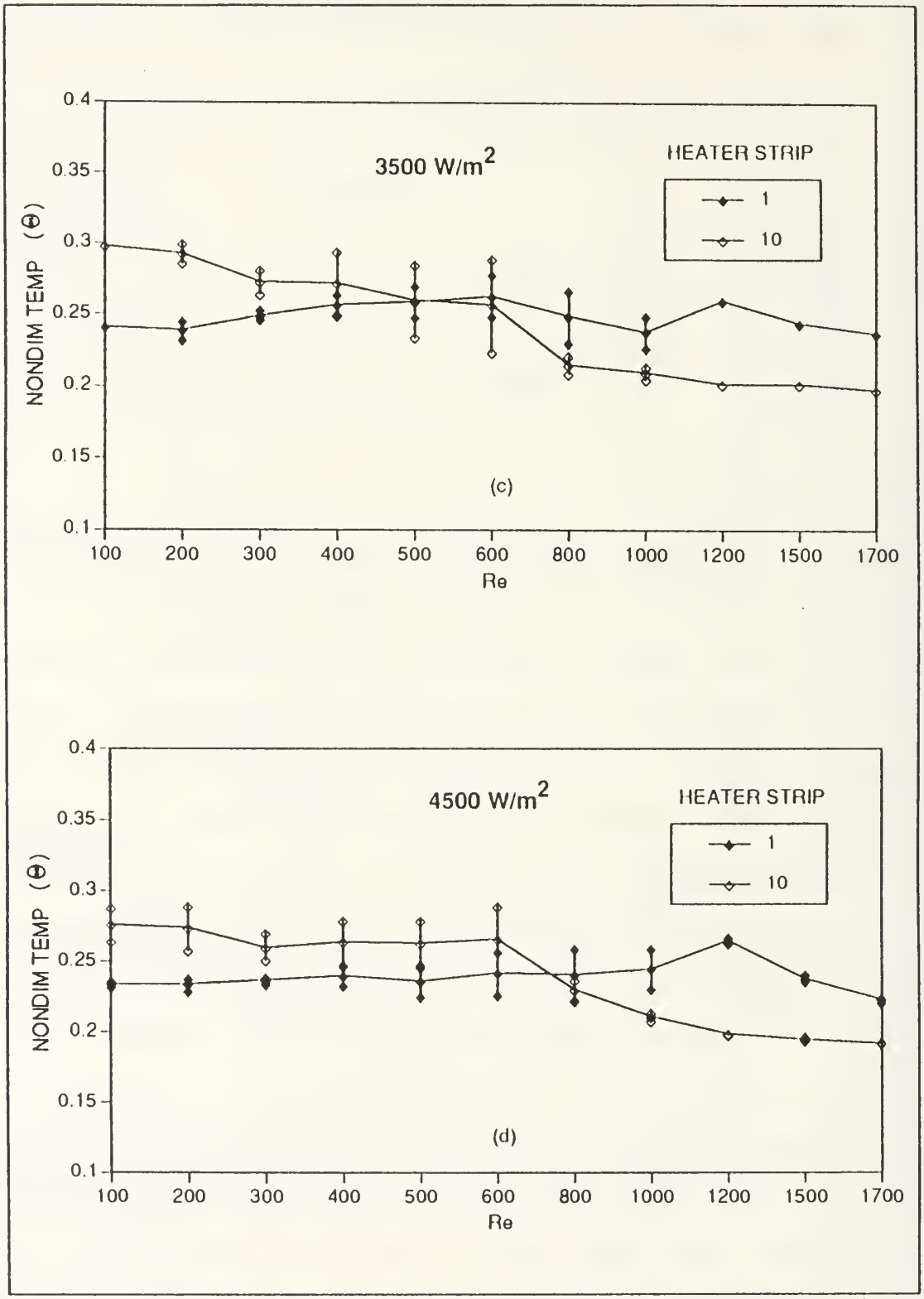

Figure 9c,d. Nondimensional Temp vs Re for opposed mixed convection at HS1 and 10 for q"=3500 and 4500 W/m^2.

for q″ = 3500 and 4500 W/m^2 do suggest trends similar to lower q″ data, but additional data runs with Re > 1700 are needed for completeness.

With the present Nusselt number data of Figures 8a-d, a power law curve fit was performed. Table III presents the exponent (n) in the correlation Nu = Constant*Re^n for the various heaters.

Looking at the columns for each heat flux shows the collapsing of the data in the forced convection dominated regime.

TABLE III. EXPONENT 'n' FOR THE POWER LAW CURVE FIT OF FIGURES 8a-d IN THE FORCED CONVECTION REGIME

HEATER STRIP	1050 W/m^2 Gr^*=70.0k Re ≥ 500	2500 W/m^2 Gr^*=166.7k Re ≥ 800	3500 W/m^2 Gr^*=233.4k Re ≥ 1200	4500 W/m^2 Gr^*=300k Re ≥ 1200
1	0.274	0.182	0.281	0.483
3	0.229	0.167	0.227	0.373
5	0.204	0.140	0.180	0.577
7	0.166	0.110	0.132	0.175
9	0.122	0.130	0.086	0.104

Figures 10a-c illustrate the effect of position on the Nusselt number. These figures show the cross over point shifting to the right from HS10 to HS1. This trend is similar to that seen in Figures 8a-d. At lower Re the flow is natural convection dominated, therefore as q″ increases Nu increases and this is seen in Figures 10a-c. For high Re, Nu = f(Re) and we see a collapsing of the data. This collapse is less noticeable for HS1 than it is for HS10 because of the effect of upstream heater strips on downstream strips.

D. OPPOSED MIXED CONVECTION LIQUID CRYSTAL VISUALIZATION

The surface temperature pattern was visualized (Figure 11) using a liquid crystal sheet which displayed shades of green and blue in the temperature range of 30 to 35 °C.

Plumes were visible for q″=3500 and 4500 W/m^2 and evident on all heaters for Re > 600. These plumes appeared to start near the bottom heaters (HS1-4) at very regular spacings and move up along the surface. Near the top heaters, the plumes were considerably wider and interaction effects were evident. Time-wise meandering of the plumes in the spanwise direction was observed.

At HS9, the plume showed no distinct streaks, it appeared as one continuous plume. Above HS10, thermals appeared. A thermal is a discrete buoyant mass of fluid ascending or descending in an ambient medium due to a difference in density [Ref 17: p. 691]. Distinct aperiodic movements were

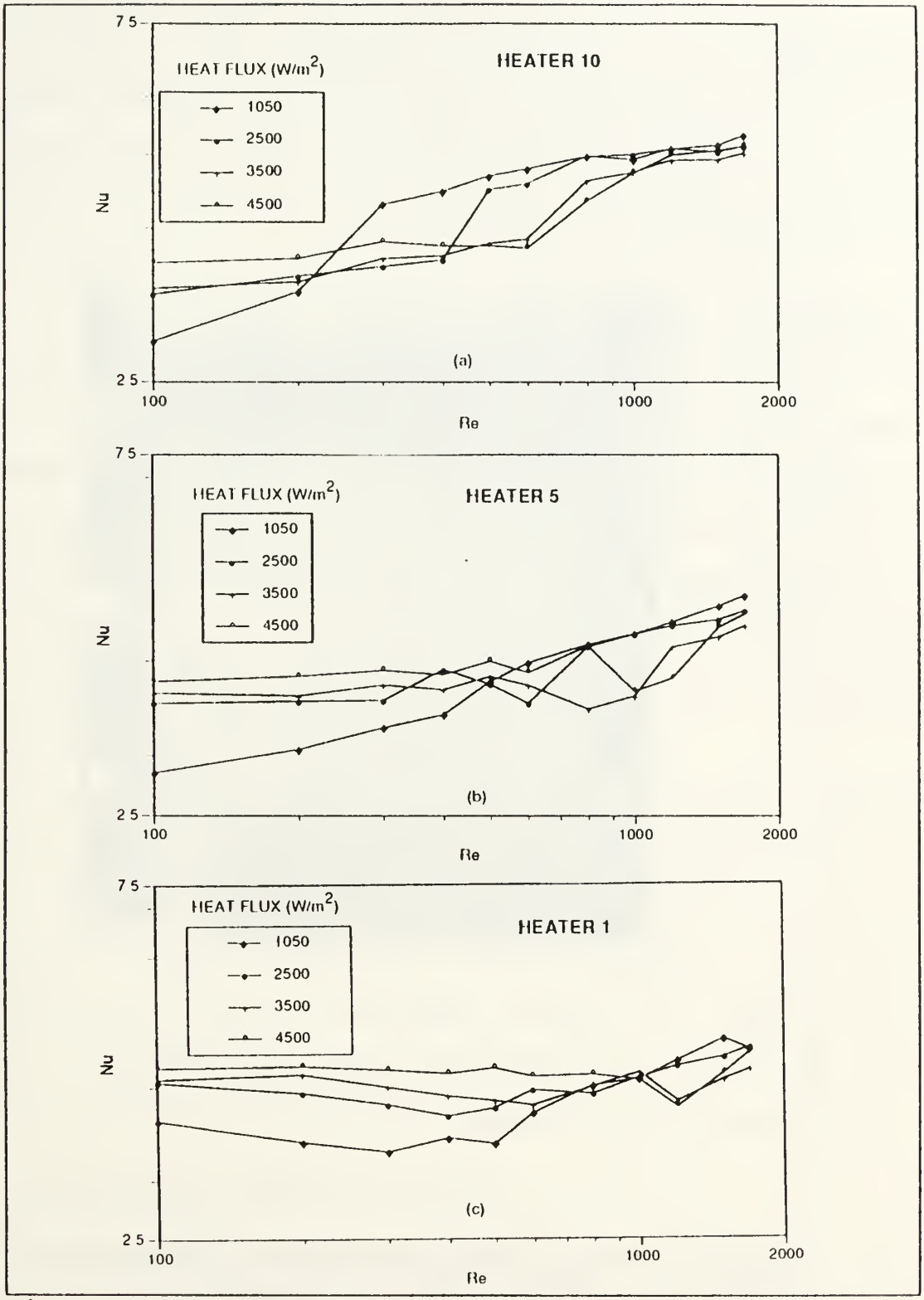

Figure 10a-c. Nu vs Re for opposed mixed convection at three different heater positions.

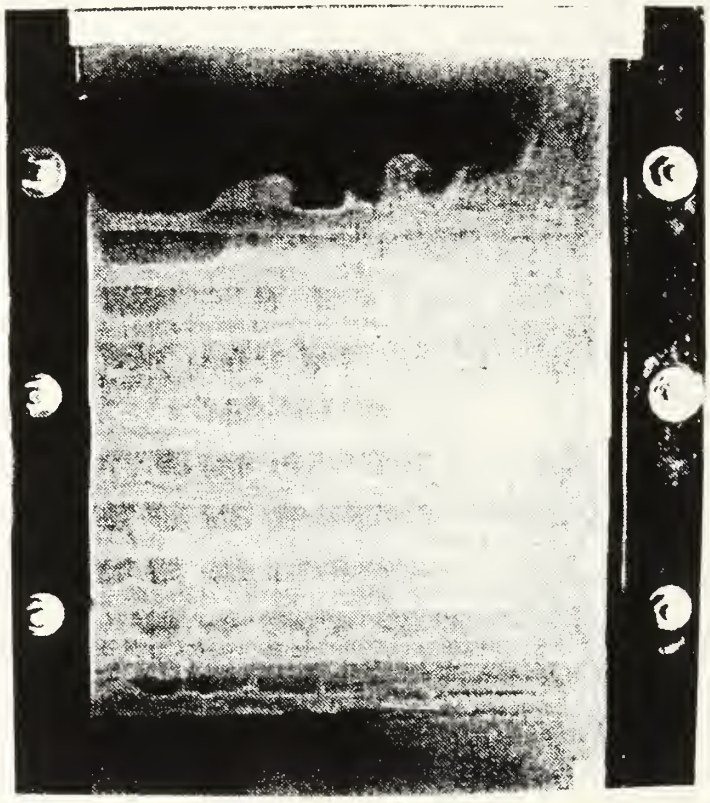

Figure 11. Liquid crystal flow visualization at $q''=3500\ W/m^2$ and Re=400.

visualized as the thermals developed. The development sequence started at an arbitrary location on HS10, grew into a mushroom like form, necked and then dissipated away. This sequence continued to repeat itself at various locations on the heater strip.

As flow increased, the height of the mushroom decreased and spanwise spacing between the individual plumes near the bottom heaters decreased. At higher flow rates where forced convection dominated, the formation of thermals ceased. Additionally, visualization of thermal plumes faded away and at Re = 1700 none were visible. For lower flow rates (Re < 300), the thermals would mingle together and at the top of the test section form into a continuous plume that gradually dissipated some distance above HS10.

The observed liquid crystal visualization agreed quantitatively with the periodic and aperiodic oscillations on the Delta Temp vs Time plots (Figures 8a-d). At low Re, buoyancy forces dominated and ΔT showed no time-wise fluctuations. As Re increased, instability ensued until forced convection flow was established--one heater at time starting with the heater strip closest to the inlet flow.

E. AIDING MIXED CONVECTION RESULTS

The same four heat flux settings and eleven Re values used for opposed mixed convection were used to analyze aiding mixed convection. Plots to be presented and discussed are: Nu vs

Re for odd heaters and HS1, 5, and 10. The results for aiding convection showed a general increase in Nu with Re. In Figures 12a-d, several trends are noticed. First, there is a decrease in slope for all heater strips as heat flux increases. The largest decrease occurs for HS1 and 3 (those closest to the inlet flow). Table IV collects the power law curve fit exponent (n) in the relationship: $Nu=Constant*Re^{n}$.

TABLE IV. EXPONENT 'n' FOR THE POWER LAW CURVE FIT OF FIGURES 11a-d IN THE FORCED CONVECTION REGIME

HEATER STRIP	1050 W/m^2 Gr^*=70.0k Re ≥ 800	2500 W/m^2 Gr^*=166.7k Re ≥ 800	3500 W/m^2 Gr^*=233.4k Re ≥ 800	4500 W/m^2 Gr^*=300k Re ≥ 800
1	0.269	0.131	0.117	0.096
3	0.260	0.139	0.123	0.102
5	0.265	0.153	0.130	0.115
7	0.254	0.157	0.130	0.108
9	0.222	0.154	0.128	0.109

Table IV does not show a collapse of the data at higher Re; but rather an asymptotic trend in the downstream direction for each q″. Secondly, at lower Re, Nu increases for all heater strips as q″ increases. This was expected since in the

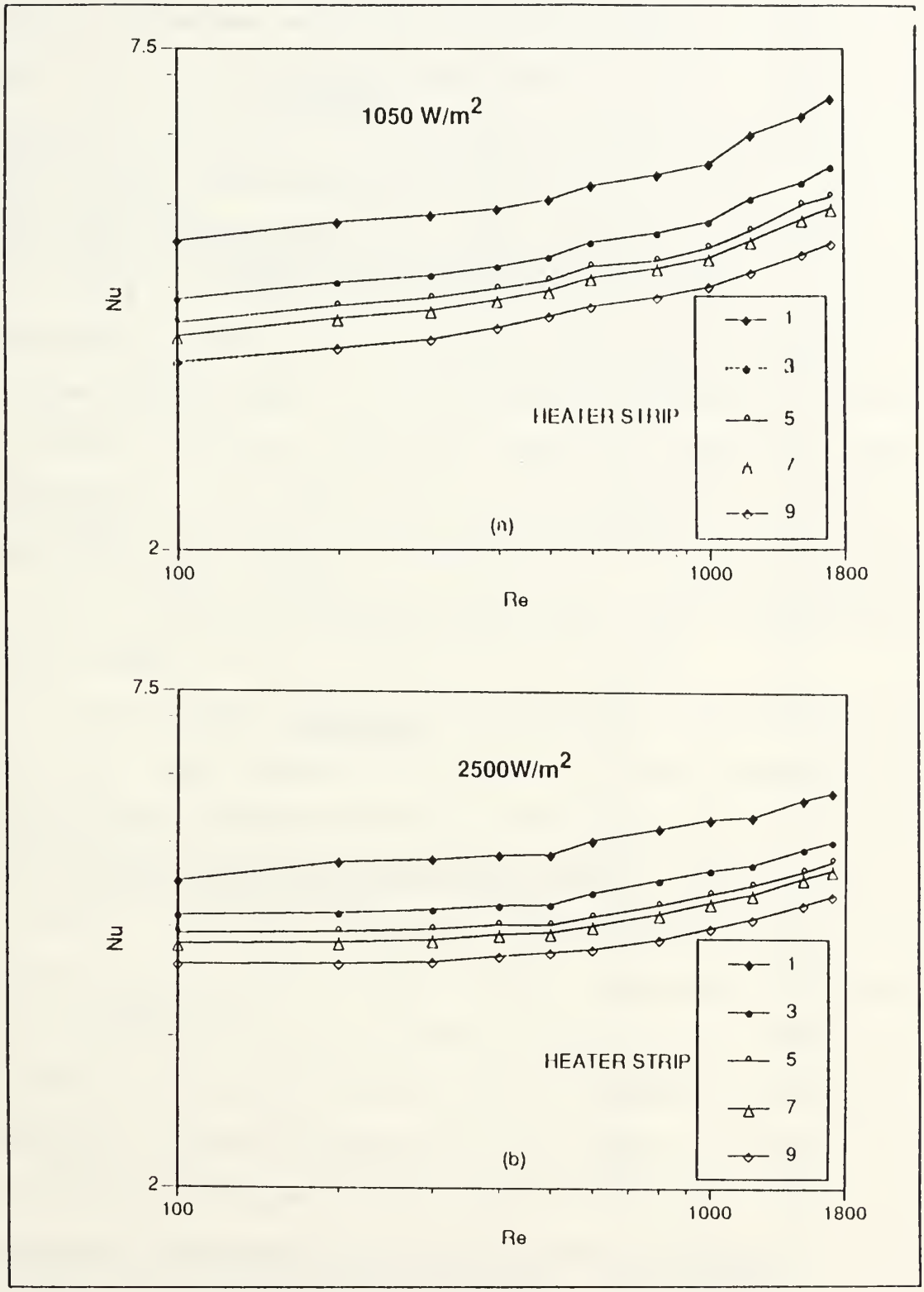

Figure 12a,b. Nu vs Re for aiding mixed convection for q"=1050 and 2500 W/m^2.

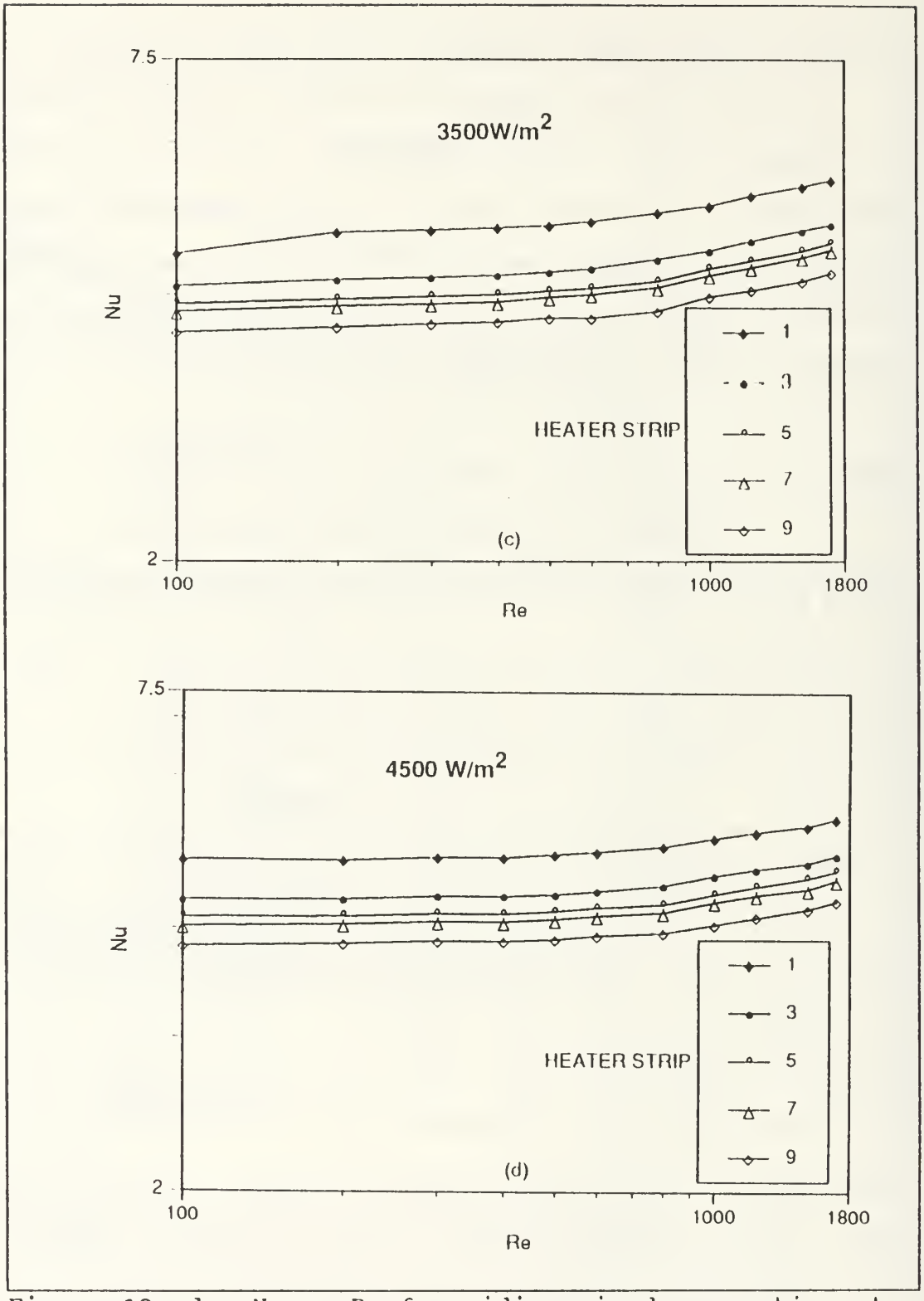

Figure 12c,d. Nu vs Re for aiding mixed convection at q"=3500 and 4500 W/m^2.

buoyancy dominated region Nu = f(Gr) and Gr^{*} = f(q″). At higher Re, in the forced convection dominated regime, the change in Nu decreases. This effect is barely noticeable for heater strips far downstream (HS7,9) at q″ = 3500 and 4500 W/m^2. This suggests that Nu = f(Re) and is not dependent on heat flux. Finally, the downstream increase in heater temperatures results in a decrease in the Nusselt numbers.

Figures 13a-c show a buoyancy dominated regime at low Re and forced convection dominated regime at high Re. This figure clearly shows the decrease in Nu downstream, and gives a better visualization of reduced heat transfer due to the cumulative thermal boundary layer buildup effect on downstream heater strips.

At first glance, Figure 13a is confusing. At low Re, the plot is what was expected (ie. higher q" yields increased Nu due to larger buoyancy forces). At higher Re, the Nu for q″=1050 W/m^2 exceeds all other heat fluxes. Wilks [Ref 18: pp. 743-752] discusses the effect of buoyancy forces on the boundary layer along a semi-infinite constant heat flux vertical plate. At the leading edge, forced convection dominates and buoyancy effects are of secondary importance. At positions further downstream, this trend is reversed and buoyancy forces dominate over forced convection. Figure 14 uses Wilks' correlation for the local Nusselt number (Pr = 1)

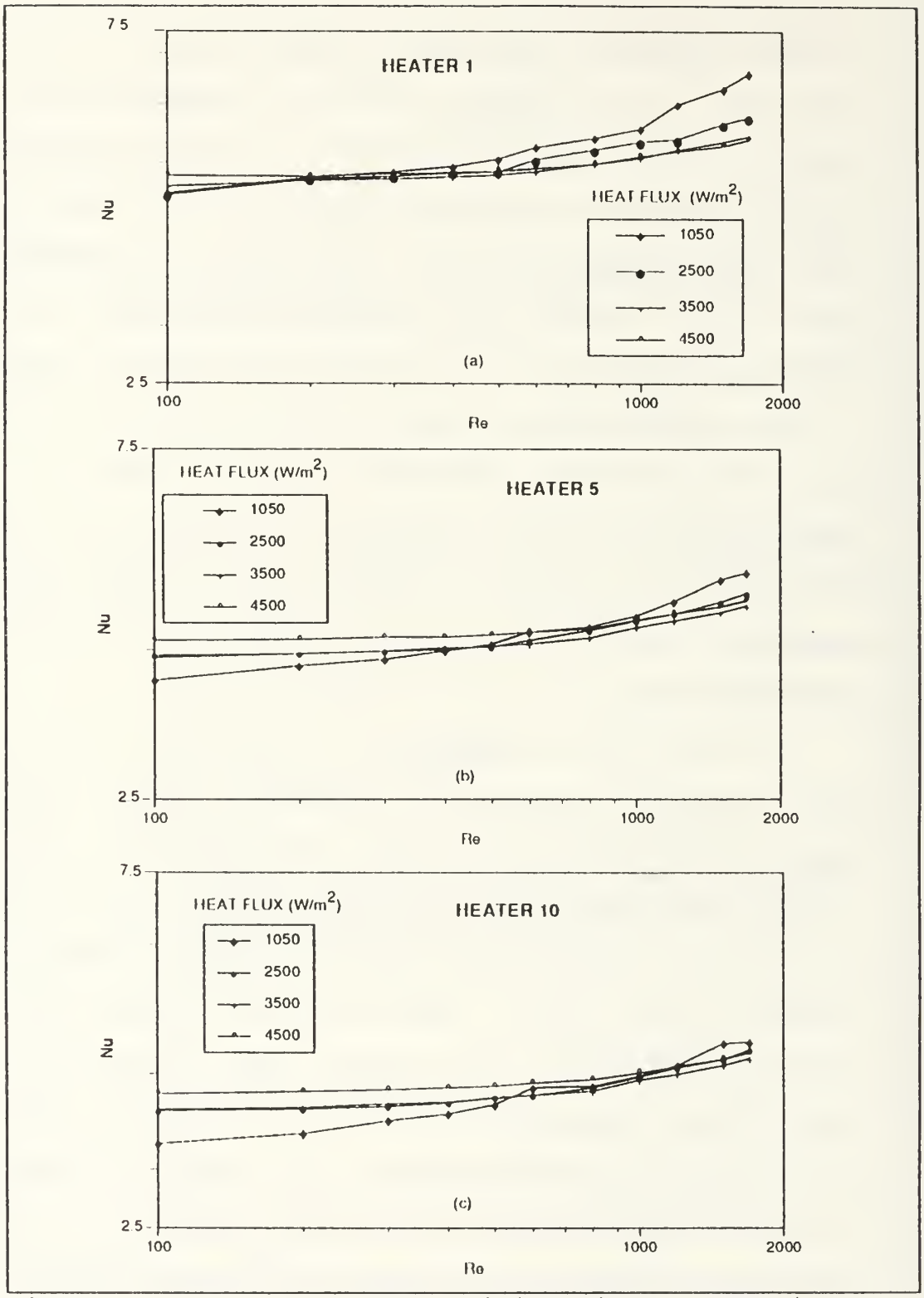

Figure 13a-c. Nu vs Re for aiding mixed convection at various heater positions.

$$Nu_x = \sqrt{Re_x}\sqrt{\epsilon}\ Q^*(\epsilon)$$

to suggest an explanation for the trend observed in Figure 13a. $Q^*(\epsilon)$, in the equation above, is the result of the full numerical integration of the boundary layer equation in Table 3 of Reference [18]. Figure 14 also shows that the Nusselt number for q"=1050 W/m^2 is smaller than for q"=4500 W/m^2 at lower Re. At higher Re, this trend is reversed.

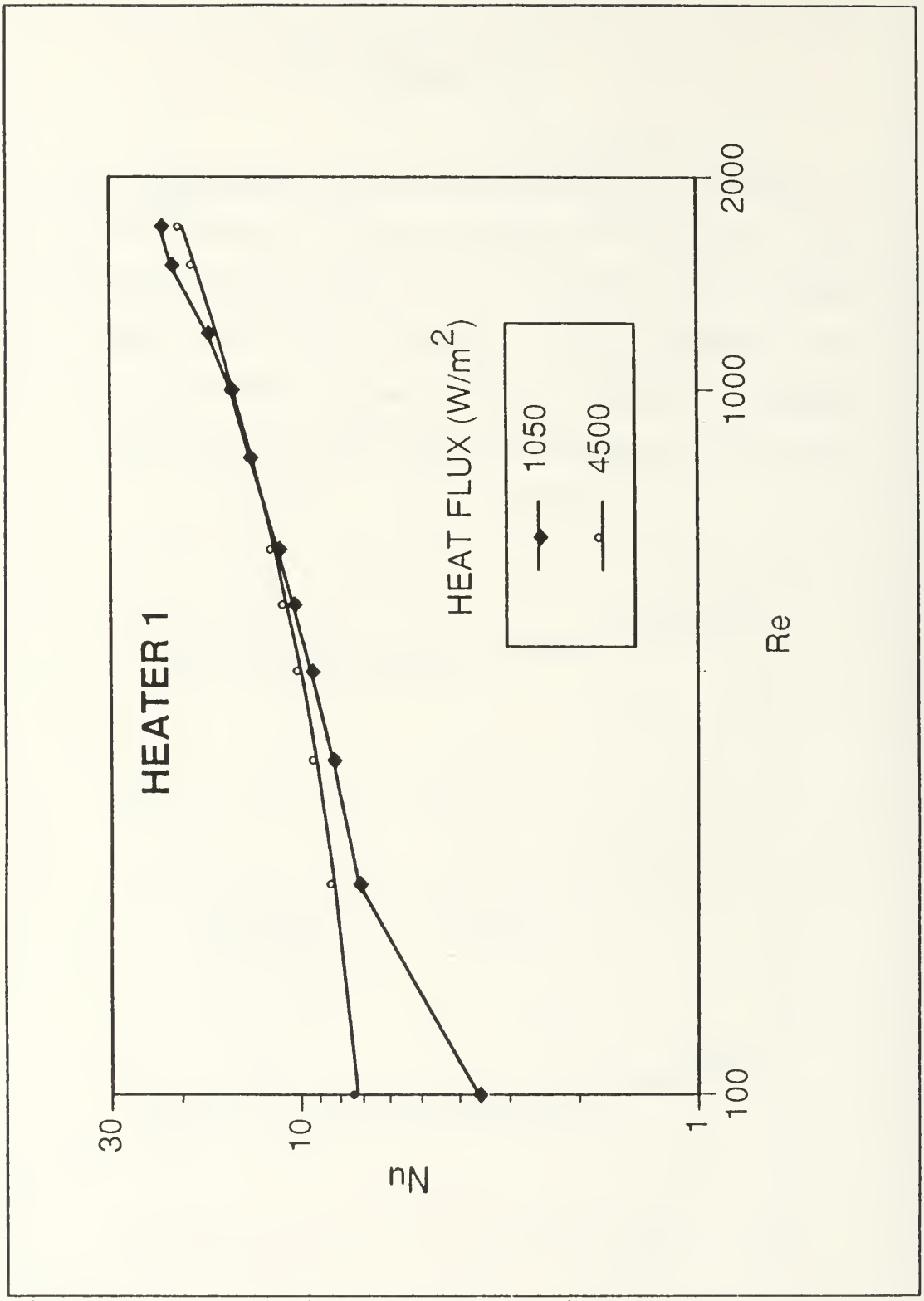

Figure 14. Comparison of HS1 at different heat fluxes using Wilks' correlation Ref[18].

IV. CONCLUSIONS

This study reached the following conclusions on the influence of flow rate, heat flux and position on convective heat transfer from discrete heat sources in a liquid filled vertical channel.

For forced convection dominated regime under both opposed and aiding conditions:

- As flow rates increased, Nusselt numbers increased.
- Heat transfer rates of downstream heaters were reduced as a result of lying in the thermal wake of upstream heaters. This was due to the cumulative buildup of the thermal boundary layers.

For opposed flow only, with all other parameters fixed, and q″ increased between 1050 and 4500 W/m^2, the following conclusions were drawn. At Re<500 where buoyancy forces dominate, higher heat fluxes resulted in higher Nu. For Re between 500 and 1000, Nu decreased and the upper limit of the mixed convection regime expanded from Re=500 to 1500; the lower limit showed a significantly smaller variation and was in the 200-300 range. In this range mixed convection regime, flow was unstable and Nu fluctuated. At Re>1000, a forced convection regime was found where Nu was a function of Re and independent of q″.

For aiding flow, as q″ increased between 1050 and 4500 W/m^2, Nu decreased for each heater strip and there were no

distinct regimes as there were for opposed flow. Additionally the slopes of the Nu vs Re curves decreased as q″ increased.

In general, this study showed the transition between buoyancy dominated to mixed and forced convective heat transfer to be very unstable for opposed flow, but stable for aiding flow. Additionally, for aiding flow, buoyancy forces acted to enhance the rate of heat transfer at low q″, while opposed flow acted to decrease the rate of heat transfer. This difference, however, decreased at higher heat fluxes.

V. RECOMMENDATIONS

In continuation of this study, it is recommended that follow on studies include:

- Velocity field determination using a Laser Doppler Velocimeter
- Development of a numerical model to predict the effects of various channel aspect ratios, heater strip sizes and fluids

APPENDIX A

UNCERTAINTY ANALYSIS

An uncertainty analysis was performed to evaluate the accuracy of the data in this study.

The uncertainty of a function $F = F(X_1, X_2, X_3)$, where $X_{1,2,3}$ are the independent measurements is determined by:

$$\delta F = \left[\left(\frac{\partial F}{\partial X_1} \delta X_1 \right)^2 + \left(\frac{\partial F}{\partial X_2} \delta X_2 \right)^2 + \left(\frac{\partial F}{\partial X_3} \delta X_3 \right)^2 \right]^{1/2}$$

For $F = C\ X_1^a\ X_2^b\ X_3^c$ the uncertainty can be put in the following form:

$$\frac{\delta F}{F} = \left[\left(a \frac{\delta X_1}{X_1} \right)^2 + \left(b \frac{\delta X_2}{X_2} \right)^2 + \left(c \frac{\delta X_3}{X_3} \right)^2 \right]^{1/2}$$

1. Nusselt Number Uncertainty.

$$N = \frac{hL}{\kappa}$$

and

$$\frac{\delta N_U}{N_U} = \left[\left(\frac{\delta L}{L}\right)^2 + \left(\frac{\delta h}{h}\right)^2\right]^{1/2}$$

where,

$$\frac{\delta h}{h} = \left[\left(\frac{\delta Q}{Q}\right)^2 + \left(\frac{\delta A}{A}\right)^2 + \left(\frac{\delta \Delta T}{\Delta T}\right)^2\right]^{1/2}$$

For

Q = 2.100 W	δQ = 0.0001 W
A = 0.002 m^2	δA = 2.50E-7 m^2
ΔT = 3.4 °C	δΔT = 0.05 °C
L = 0.01 m	δL = 0.0005 m
κ = 0.613 W/m K	
h = 308.82 W/m K	
Nu = 5.04 ± 0.26	

The uncertainty δNu/Nu = 0.052 or 5.2%.

2. Reynolds Number Uncertainty.

$$Re = \frac{U_m D_h}{\nu}$$

$$\frac{\delta R_E}{R_E} = \left[\left(\frac{\delta U_M}{U_M}\right)^2 + \left(\frac{\delta D_H}{D_H}\right)^2\right]^{1/2}$$

where,

$$\frac{\delta D_H}{D_H} = \left[\left(\frac{\delta A}{A}\right)^2 + \left(\frac{\delta P}{P}\right)^2\right]^{1/2}$$

For

$A = 0.002\ m^2$	$\delta A = 2.5e\text{-}7\ m^2$
$P = 0.42\ m$	$\delta P = 0.0005\ m$
$U_m = 0.0767\ m/s$	$\delta U_m = 0.005\ m/s$
$\nu = 0.857E\text{-}6\ m^2/s$	
$Re = 1700 \pm 111$	

The uncertainty $\delta Re/Re = 0.065$ or 6.5%.

3. Flux Based Grashof Number Uncertainty.

$$Gr^* = \frac{g\beta Q L^4}{\kappa \nu^2 A}$$

$$\frac{\delta Gr^*}{Gr^*} = \left[\left(\frac{\delta Q}{Q}\right)^2 + \left(4\frac{\delta L}{L}\right)^2 + \left(\frac{\delta A}{A}\right)^2\right]^{1/2}$$

For the same values given in subsection 1 except $\delta L=0.000127m$ and $\beta=306E\text{-}6\ K^{-1}$, $Gr^* = 70{,}009 \pm 3{,}570$.

The uncertainty $\delta Gr^*/Gr^* = 0.051$ or 5.1%.

APPENDIX B

SAMPLE CALCULATIONS

The following calculation is for HS9 where q''=1050 W/m^2, Re=1700, T_{IN}=26.85 °C and ΔT=3.4 °C.

1. Characteristic Dimensions.

Perimeter (P) = 2(0.2 + 0.01)

= 0.42 m

Heater surface area (A_s) = (0.20)(0.01)

= 0.002 m^2

Channel cross sectional area (A_c) = (0.02)(0.01)

= 0.002 m^2

Hydraulic diameter (D_H) = 4(0.002)/0.42

= 0.019 m

2. Convective Heat Flux.

Power to heater = 2.100 W

Heat flux (Q'') = 2.100/0.002

= 1050 W/m^2

3. Water Properties [Ref 8: p. A22].

β = 306E-6 K^{-1}

ν = .857E-6 m^2/s

κ = 0.613 W/m·K

4. Reynolds Number.

Re = $U_m D_H/\nu$

=(0.0767)(0.019)/0.857E-6 = 1700

5. **Heat Transfer Coefficient.**

$h = q''/\Delta T$

$= 1050/3.4$

$= 308.8\ W/m^2 \cdot K$

6. **Nusselt Number.**

$Nu = hL/\kappa$

$= 308.8(0.01)/(0.613)$

$= 5.04$

7. **Fluxed Based Grashof Number.**

$Gr^* = g\beta q'' L^4/\kappa\nu^2$

$= (9.81)(306E-6)(1050)(0.01)^4/(0.613)(0.857E-6)^2$

$= 70,009$

LIST OF REFERENCES

1. Joshi, Y.K. and Kelleher, M.D., "Liquid Cooling of Electronic Equipment," Naval Research Review, v. 1, 1992.

2. Chu, R.C., "Heat Transfer in Electronic Systems." The 8th International Heat Transfer Conference Proceedings, v.I, 1986.

3. Tuckerman, D.B. and Pease, R.F., "High-Performance Heat Sinking for VLSI," IEEE Electronic Device Letters, v. EDL-2, No.5, pp. 126-129, May 1981.

4. Park, K. and Bergles, A., "Natural convection Heat Transfer Characteristics of Simulated Microelectronics Chips," ASME Journal of Heat Transfer, v. 109, pp. 90-96, 1987.

5. Keyhani, M., Prasad, V. and Cox, R., "An Experimental Study of Natural Convection in a Vertical Cavity with Discrete Heat Sources," ASME Journal of Heat Transfer, v. 110, pp. 616-623, Aug 1986.

6. Kishimoto, T. and Sasaki, S., "Cooling Characteristics of Diamond-Shaped Interrupted Cooling Fin for High-Power LSI Devices," Electronic Letters, v. 23, pp. 456-457, Apr 1987.

7. Phillips, R.J., Glicksman, L.R. and Larson, R., "Forced-Convection, Liquid-Cooled, microchannel Heat Sinks for High-Power-Density Microelectronics," Proc. Inl. Symp. on Cooling Technology for Electronics Equipment, Honolulu, HI, pp. 227-248, Mar 1987.

8. Phillips, R.J., "Microchannel Heat Sinks," The Lincoln Laboratory J, v. 1, pp. 31-48, Spring 1988.

9. Cheng, C-H., Kou, H-S. and Huang, W-H., "Flow Reversal and Heat Transfer of Fully Developed Mixed Convection in Vertical Channels," Journal of Thermophysics, v. 4 (3), p. 375, Jul 1990.

10. Mahaney, H.V., Incopera, F.P. and Ramadhyani, S., "Comparison of Predicted and Measured Mixed Convection Heat Transfer from an Array of Discrete Sources in a

11. Mori, Y. and Ohbuchi, M., "A Fundamental Study of Flow and Heat Transfer Performances of Downward Water Flow at Low Reynolds Numbers in a Vertical Heated Straight Tube," International Journal of Heat and Mass Transfer, v. 32 (3), 1989.

12. Syring, J.D., "Mixed and Forced Convection from an Array of Discrete Heat Sources in a Vertical Channel," Master's Thesis, Naval Postgraduate School, Monterey, CA, Mar 1992.

13. Schlichting, H., Boundary-Layer Theory, 7th ed., McGraw-Hill, Inc, 1979.

14. Baker, E., "Liquid Immersion Cooling of Small Electronic Devices," Microelectrons and Reliability, v. 12, 1973.

15. Kays, W.M. and Crawford, M.E., Convective Heat and Mass Transfer, McGraw-Hill Publishing Company, 1980.

16. Joshi, Y. and Knight, D.L., "Natural Convection from a Column of Flush Heat Sources in a Vertical Channel in Water," Journal of Electronic Packaging, v. 112, Dec 1990.

17. Gebhart, B., et al, Buoyancy-Induced Flows and Transport, Hemisphere Publishing Corp., 1988.

18. Wilks, G., "The Flow of a Uniform Stream over a semi-infinite Vertical Plate with Uniform Surface Heat Flux," International Journal of Heat and Mass Transfer, v. 17, 1974.

INITIAL DISTRIBUTION LIST

		Copies
1.	Defense Technical Information Center Cameron Station Alexandria, Virginia 22304-6145	2
2.	Library, Code 52 Naval Postgraduate School Monterey, California 93943-5002	2
3.	Prof. Matthew D. Kelleher Code ME/Kk Department of Mechanical Engineering Naval Postgraduate School Monterey, California 93943-5002	1
4.	Prof. Y. Joshi, Code ME/Ji Department of Mechanical Engineering Naval Postgraduate School Monterey, California 93943-5002	2
5.	Mr. Kip Hoffer Naval Weapons Support Center Code 6042 Crane, Indiana 47522	1
6.	Mr. Tony Buechler Naval Weapons Support Center Code 6042 Crane, Indiana 47522	1
7.	Naval Engineering Curricular Officer, Code 34 Naval Postgraduate School Monterey, California 93943-5002	1
8.	Ronald G. Rahall 2330 S. Rolfe St Arlington, Virginia 22202	1

Thesis
R1414 Rahall
c.1 Convective heat transfer from discrete heat sources in a liquid filled vertical channel.